3. EPICENTRAL REGION

This chapter summarizes the observations made by GEER Team members on the geotechnical/geological aspects of the M_w5.8 Mineral, Virginia earthquake of 23 August 2011 in the epicentral region. Within hours of the event, members of the team arrived in the epicentral region (i.e., Louisa County, Virginia) to document perishable data that potentially could be used to advance the geo-engineering profession's understanding of the geotechnical/geological aspects of earthquakes in general, and of intra-plate earthquakes more specifically. The team focused on documenting tectonically/seismically-induced ground deformations, evidence of liquefaction and lateral spreading, land/rock slides, ground subsidence, performance of earthen dams, damage to building foundations, and damage to public infrastructure and lifelines, among other effects of the earthquake. The team began collecting data on the night of the main shock (i.e., 23 August 2011) and continued for several months thereafter, with the majority of effort being concentrated in the few days immediately following the main shock. The documentation of the data following the event was time critical because of the heavy rains and river flooding associated with Hurricane Irene that was forecast to impact the area on 27 August 2011, with the rains and flooding having the potential to significantly modify or destroy the geotechnical/geological effects of the earthquake. To maximize the efficiency of the team's efforts, team members met several times with the personnel staffing the Emergency Operations Center (EOC) in Louisa to obtain damage reports which were used to coordinate the team's field surveys.

The Team's observations are organized in the following categories: Ground Failures (liquefaction, river bank slumps, subsidence, and rockfalls); Lifelines (bridges, power, water, and railroad); Dams, Landfill, Schools, and Foundations/Buildings.

Ground Failures

Liquefaction

The soils in Louisa County are largely residual clay, so it was not expected that liquefaction would be pervasive during this event. However, the Team did search in low lying areas where the ground water table was expected to be high and where there was a possibility of the presence of liquefiable deposits (e.g., floodplains). In total, four small liquefaction sand boils were found at the locations marked in Figure 1, with photos of the features shown in Figure 2 (Note that the two features in the S. Anna River bed were found by Jeff Munsey, TVA, and the nearby feature on the roadside was found by Ed Harp, USGS). Also shown in Figure 1 are the epicentral locations of the main shock and aftershocks that were greater than M_w3.0 that occurred within two days of the main shock. Assuming that these epicenters define the general location/orientation of the rupture plane of the main shock, it can be inferred from Figure 1 that the liquefaction features lie approximately above the rupture plane. It is possible that liquefaction occurred in other areas, but the undergrowth in the region is so thick and

sand deposits so sparse, no other features were found despite an extensive search along streams and in floodplains in the epicentral region. Also, there were several heavy rains in the days and weeks after the main shock that resulted in high river levels, which likely washed away any features in the river and creek beds.

The liquefied soil was coarse sand, with the feature in the drainage channel containing some plasticity. No feeder dikes could be found for the features in the S. Anna River riverbed (Figure 2b), but the riverbed was very gravelly and the water table was only an inch or two below the ground surface. As a result, a clean cut could not be made vertically through the feature and the cut quickly filled with water. The features on the roadside (Figures 2c,d) and the feature in the drainage channel in the woods (Figures 2e,f) both appeared to have vented through existing animal holes or burrows.

Figure 1. Aerial image of the epicentral region showing locations of observed liquefaction sand boils. Also shown in this image are the epicenters of the main shock and aftershocks that occurred within two days of the main shock that had magnitudes greater than 3.0.

(a) (source: Mark Carter, USGS)

(b)

(c)

(d)

(e)

(f)

Figure 2. Liquefaction sand boils found in the epicentral region: (a) two sand boils in the S. Anna River riverbed near Yancy Mill (features found by Jeff Munsey, TVA) (37.93839, 77.98269); (b) cross-sectional cut through one of the sand boils in the S. Anna River riverbed. The trowel points to a layer of leaves, indicating that the blow material was recently placed; (c) sand boil found across the road from the features in the riverbed (feature found by Ed Harp, USGS) (37.93807, -77.98238); (d) horizontal cut through the roadside feature showing a plan view of the feeder dike; (e) sand boil found in a drainage channel in the woods of Bend

of River Rd (37.95668, -78.00502); (f) horizontal and vertical cut through the drainage channel feature.

On 25 August 2012, geologists F. Syms and R. Cumbest, Fugro Consultants, Inc., conducted a low altitude over flight of the epicentral region. As shown in Figure 3, the flight path originated in Chesterfield, VA (just south of Richmond) and included the James and Rivanna Rivers, epicentral region, and the western edge of Lake Anna. No evidence of surface deformation in the epicentral and surrounding region was noted. Numerous point bars (e.g., Figure 4), river and lake banks, open crop fields, were observed with no signs of liquefaction, lateral spread or surface offset. The vegetation over smaller creeks prevented any observations.

Figure 3. Low altitude flight path of geologists F. Syms and R. Cumbest conducted on the morning of 25 August 2012. (courtesy of F. Syms)

Figure 4. Aerial photo of point bar along Rivanna River near Palmrya, VA, approximately 27 km from the epicenter. No evidence of liquefaction or lateral spreading was observed. (courtesy of F. Syms)

Samples of liquefaction ejecta were collected from both liquefaction sites for grain size analyses. Figure 5 shows the grain size distribution curves for the samples. The ejecta from the features at the Yanceyville mill site (Yancey-3) classified as SW-SM: Well-graded Sand with Silt and Gravel per the ASTM-2487 soil classification system (ASTM 2011). Because the ground surface layer at this site was very gravelly and the water-table was only several centimeters below ground surface, a clean cut could not be made vertically through the feature and the cut that was made quickly filled with water. As a result, feeder dikes for the features could not be found (Figure 2a,b). The ejecta sample from the Bend of the River site (BOR-2) was much finer than that from the Yancey-3 site and classified as ML: Silt per the ASTM-2487 soil classification system (ASTM 2011). The feature at the Bend of River site (Figures 2e,f) appeared to have vented through an existing animal or root hole, and it is likely that the feature would not have manifested on the ground surface in the absence of the pre-existing hole. Finally, superimposed on the grain distribution plot are the bounds proposed by Tsuchida (1970) for the grain size ranges for soils that are “most susceptible to liquefaction” and “potentially susceptible to liquefaction”. While grain size distribution is only one aspect influencing the liquefaction susceptibility of a soil stratum, it can be seen that the samples from the Yancey-3 and BOR-2 sites generally fall outside the “most susceptible to liquefaction” boundaries, but do generally fall within the boundaries for “potentially susceptible to liquefaction”.

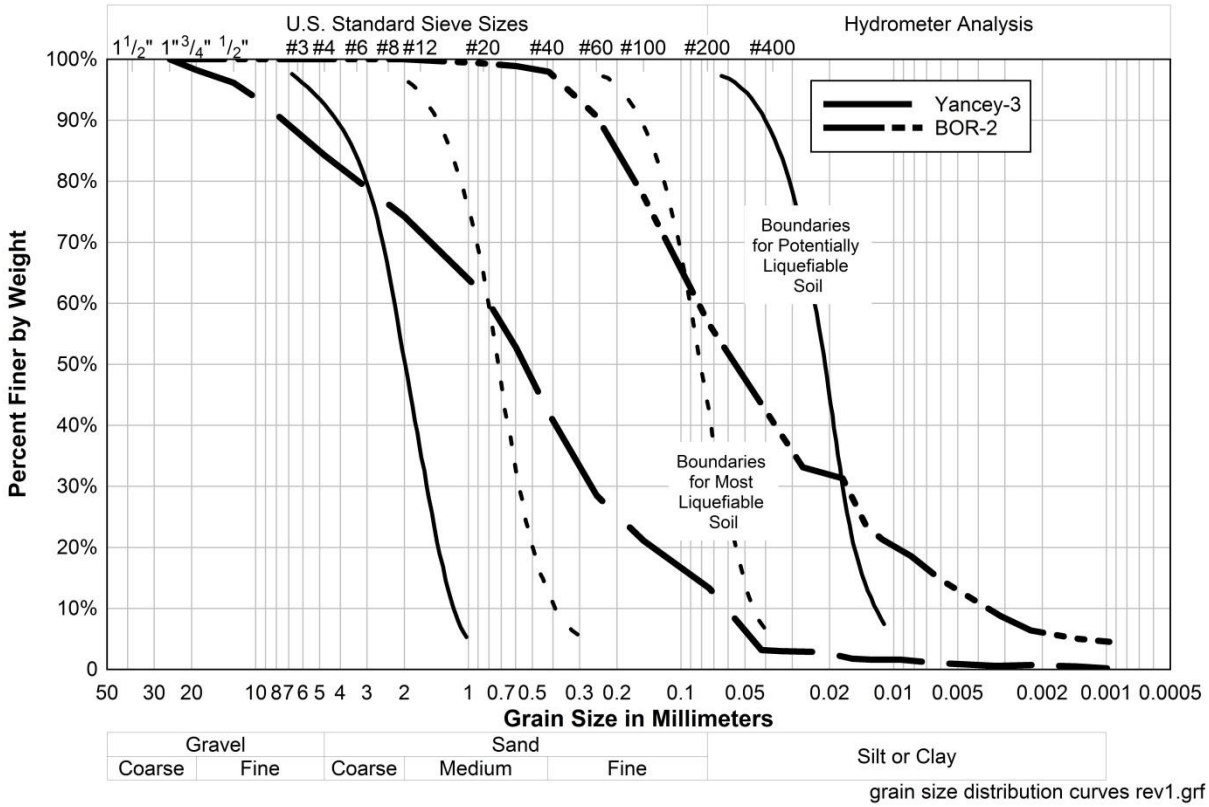

Figure 5. Grain size distribution curves for the liquefaction ejecta samples. Superimposed on the grain distribution plot are the bounds proposed by Tsuchida (1970) for the grain size ranges for soils that are "most susceptible to liquefaction" and "potentially susceptible to liquefaction".

In addition to grain size analyses, dynamic cone penetration (DCP) tests were performed at the two liquefaction sites. The DCP used for this study was designed by Professor George Sowers (Sowers and Hedges, 1966) and is shown in Figure 6. In addition to this earthquake, the Sowers DCP has been used on several other recent post-earthquake investigations to evaluate deposits that liquefied (e.g., the 2008, M_w6.3 Olfus, Iceland earthquake, the 2010, M_w7.0 Haiti earthquake, the 2010 Mw7.1 Darfield, New Zealand earthquake, the 2010, M_w8.8 Maule, Chile earthquake, and the 2011, M_w6.2 Christchurch, New Zealand earthquake). This system utilizes a 6.8 kg mass (15-lb drop weight) on an E-rod slide drive to penetrate an oversized 45° apex angle cone. The cone is oversized to reduce rod friction behind the tip. The DCP tests consists of counting the number of drops of the 6.8 kg mass that is required to advance the cone ~4.5 cm (1.75 inches), with the number of drops, or blow count, referred to as the DCP N-value or N_{DCPT}. N_{DCPT} is approximately equal to the Standard Penetration Test (SPT) blow count up to an N-value of about 10 (Sowers and Hedges, 1966; Green et al., 2011a,b). However, beyond an N-value of 10, the relationship becomes non-linear. The correlation relating SPT and DCP N-values used in this study is the same one used by Green et al. (2011a,b), which is a slightly modified version of the correlation proposed by Sowers and Hedges (1966).

Figure 6. Sowers Dynamic Cone Pentrometer (DCP). Used to measure in-situ properties at the Yancey-3 and BOR-2 liquefaction sites.

Following the procedure outlined in Olson et al. (2011), the SPT equivalent N-values ($N_{SPTequiv}$) values were normalized for effective overburden stress and hammer energy using the following relationship:

$$N_{1,60-SPTequiv} \approx N_{SPTequiv}(N_{DCPT}) \cdot \left(\frac{P_a}{\sigma'_{vo}} \right)^{0.5} \frac{ER}{60\%} \quad (1)$$

where $N_{SPT\ equiv}(N_{DCPT})$ is the functional relationship between N_{SPT} and N_{DCPT} mentioned above (Green et al., 2011a,b), P_a is atmospheric pressure (i.e., 101.3 kPa), σ'_{vo} is initial vertical effective stress (in the same units as P_a), and ER is energy ratio. This relationship uses the effective stress and hammer energy normalization schemes outlined in Youd et al. (2001). Although the energy ratio for the system was not measured, the DCP hammer is similar to the donut hammer used for the SPT. Skempton (1986) and Seed et al. (1984) suggested that the energy ratio for an SPT donut hammer system ranges from about 30 to 60%. However, because the DCP system does not have pulleys, a cathead, etc., we anticipate that the energy ratio for the DCP is likely to be near the upper end of this range. Therefore, we assumed an ER = 60% for our calculations.

In addition to the effective stress and hammer energy corrections, the $N_{SPT\ equiv}$ values were also corrected for fines content following the procedure proposed in Youd et al. (2001), where the fines contents were determined from the grain size distribution curves shown in Figure 5. Figure 7 shows a plot of N_{DCPT} and $N_{1,60cs\text{-}SPTequiv}$ for the two liquefaction sites identified by the ground reconnaissance team.

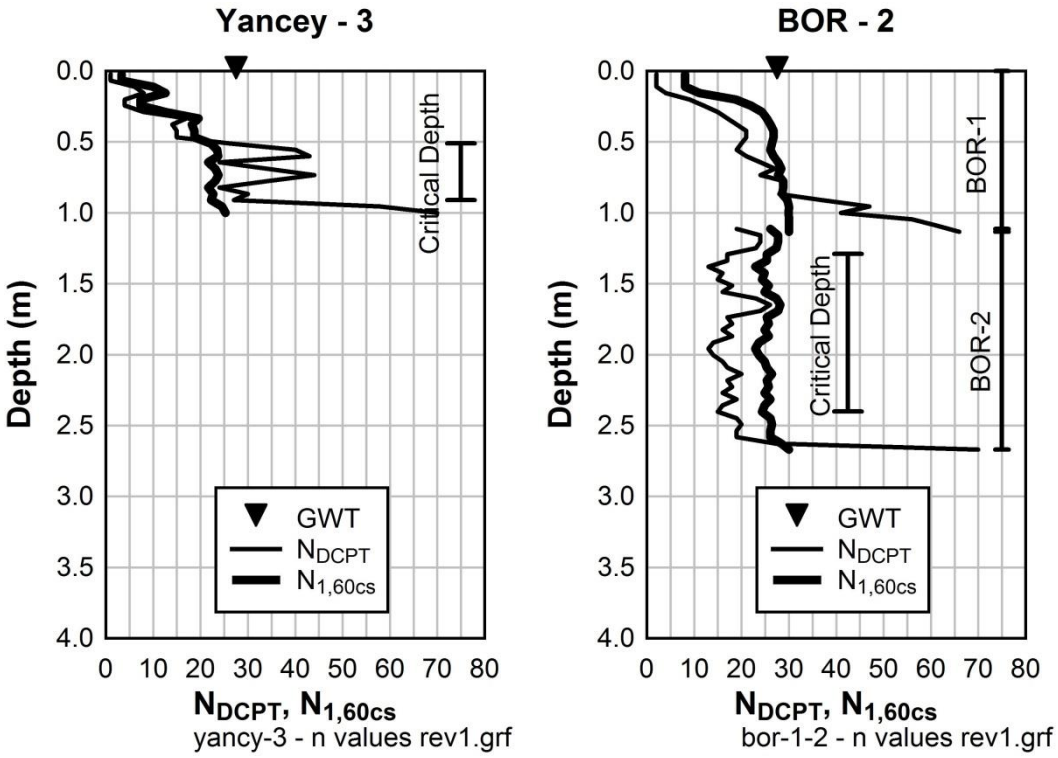

Figure 7. N_{DCPT} and $N_{1,60cs\text{-}SPTequiv}$ for the two liquefaction sites identified by the ground reconnaissance team (Yancey-3 and BOR-2).

The cyclic stress ratios (CSRs) at the DCP test sites were calculated following the methodology outlined in Youd et al. (2001), assuming the peak ground accelerations (PGA) at both sites were 0.5 g (Chapman, 2012b). The average of the recommended range of magnitude scaling factors (MSFs) proposed in Youd et al. (2001) was used to compute $CSR_{M7.5}$ at the sites. Using the $N_{1,60cs\text{-}SPTequiv}$ described above, the correlation proposed by Youd et al. (2001) was used to estimate the cyclic resistance ratio for a M_w7.5 event (i.e., $CRR_{M7.5}$). Comparisons of the computed $CSR_{M7.5}$ and $CRR_{M7.5}$ for both sites are shown in Figure 8. As shown in this figure, liquefaction is predicted to have occurred at both sites (i.e., $CSR_{M7.5} > CRR_{M7.5}$). However, the factors of safety against liquefaction (FS = $CRR_{M7.5}/CSR_{M7.5}$) are very close to 1.0 and the thicknesses of the liquefied layers are predicted to be relatively thin. These predictions are consistent with the small sand boils found at the sites. Furthermore, these analyses show that the stark contrast in the paucity of features produced by the Mineral earthquake compared to the widespread liquefaction that was caused by similar magnitude events in Christchurch, New Zealand in June 2011 is most likely due to the differences in the liquefaction susceptibility of soils in the two regions, rather than the difference in the characteristics of the ground shaking (Green and Lasley, 2012).

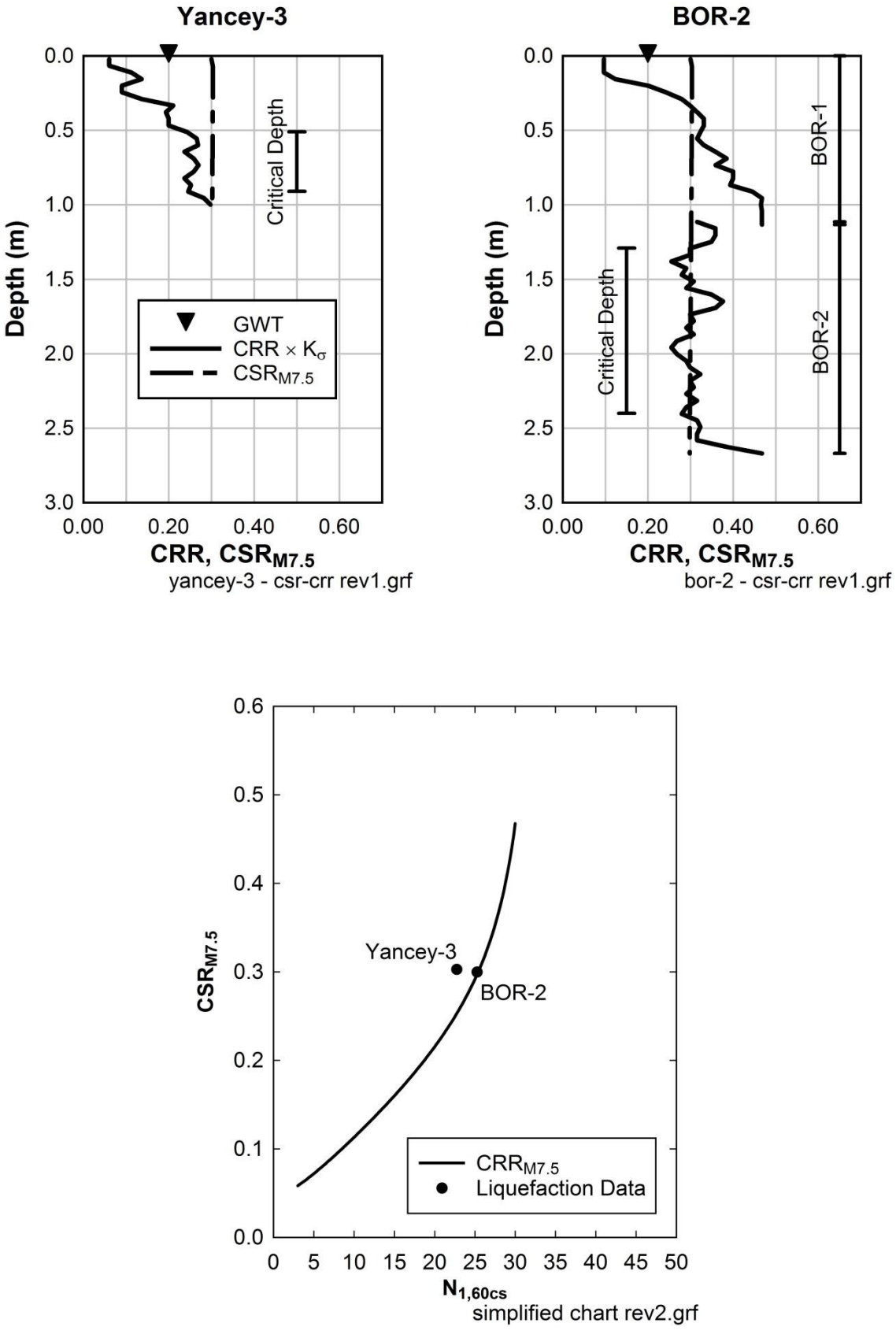

Figure 8. Results from simplified liquefaction evaluations of Yancey-3 and BOR-2 liquefaction sites.

Finally, from an engineering perspective, the observed liquefaction during the Mineral, Virginia earthquake is not significant in itself. However, it adds to the relatively limited database of earthquake-induced liquefaction in stable continental regions and is valuable in validating relationships used to estimate the magnitude of pre-instrumental and/or paleoearthquakes in the region. Towards this end, the most distal liquefaction feature from the epicenter for this event is BOR-2 site, which is ~6.25 km from the main shock epicenter. This distance is plotted in Figure 9, along with data from worldwide earthquakes compiled by Ambraseys (1988). As may be observed from this figure, the epicentral distance falls close to, but within, the boundary for maximum distance.

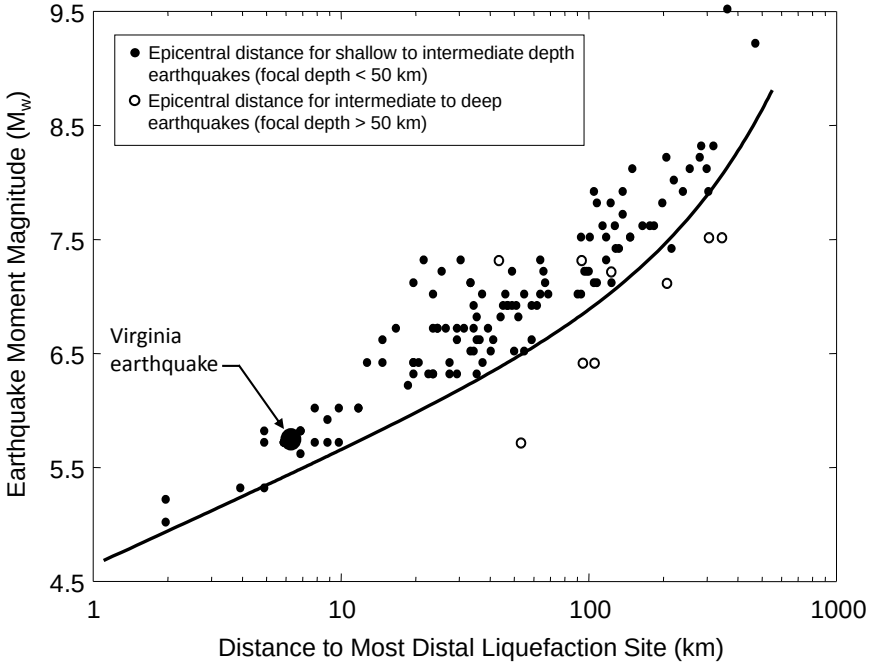

Figure 9. Comparison of the most distal liquefaction feature from the Mineral, Virginia earthquake of 23 August 2011 with worldwide earthquake data collected by Ambraseys (1988).

Riverbank Slumps

Mark Carter, USGS, searched the South Anna River for slumps in the banks. One small slump was found very close to the liquefaction features shown in Figure 2a, which again is likely located approximately over the rupture plane. This slump is shown in Figure 10. Heavy rains from Hurricane Irene started on 27 August and made it impossible to definitively attribute slumps found subsequently to earthquake shaking.

Figure 10. Slump in the bank of the S. Anna River near the Yancy Mill (37.938495, -77.983203).

Subsidence

Mark Carter, USGS, found what is believed to be earthquake-induced subsidence of an abandoned gold mine. The location of the subsidence is shown in Figure 11. A photograph of the subsidence is shown in Figure 12.

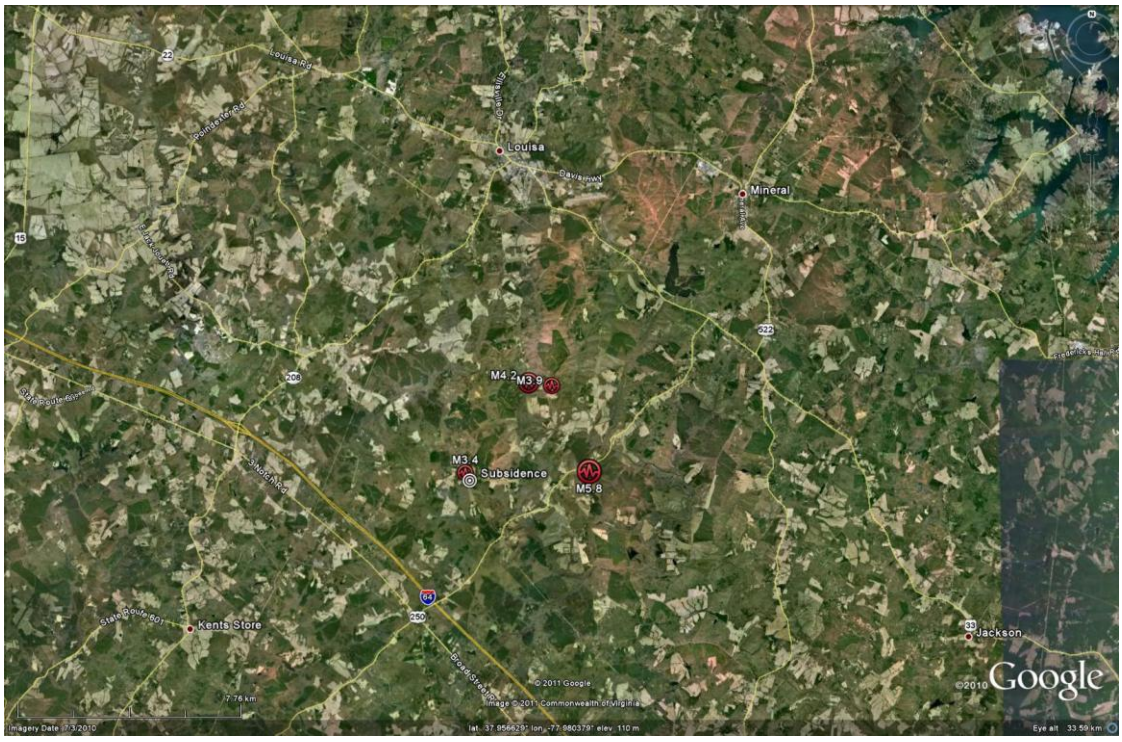

Figure 11. Aerial image showing the location of where it is believed the earthquake-caused subsidence of the ground surface above an abandoned gold mine.

(a)

(b)

Figure 12. Photograph of the area that subsided (Photo by Mark Carter) (37.9229, -78.0176).

Rockfalls

Mark Carter and Ed Harp, both of the USGS, identified four minor rock falls in the epicentral region, two along the banks of the South Anna River and two in road cuts. The locations of these rock falls are shown in Figure 13, with photographs of two of these rock falls shown in Figure 14.

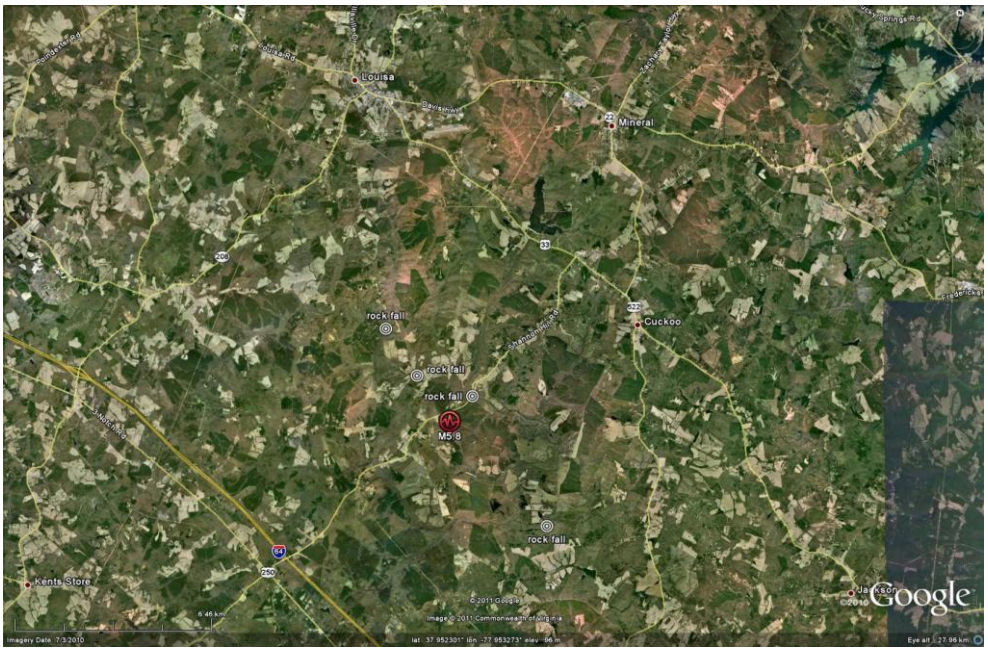

Figure 13. Locations of rock falls found in the epicentral region along the S. Anna River and road cuts.

(a) (b)

Figure 14. Rock falls found in the epicentral region (source: Mark Carter): (a) rockfall along Shannon Hill Rd (37.93174, -77.96190); and (b) rockfall along Vigor Rd, near the intersection with Yanceyville Rd (37.93802, -77.98245).

Ed Harp and Randy Jibson, both from the USGS, determined the areal extents of rockfalls to be just north of Harper's Ferry to the north, the Virginia - West Virginia border to the west, and about 10 miles north of the North Carolina border along the Blue Ridge Parkway to the

southwest. They were not able to determine the eastern limit. The determined limits are shown in Figure 15.

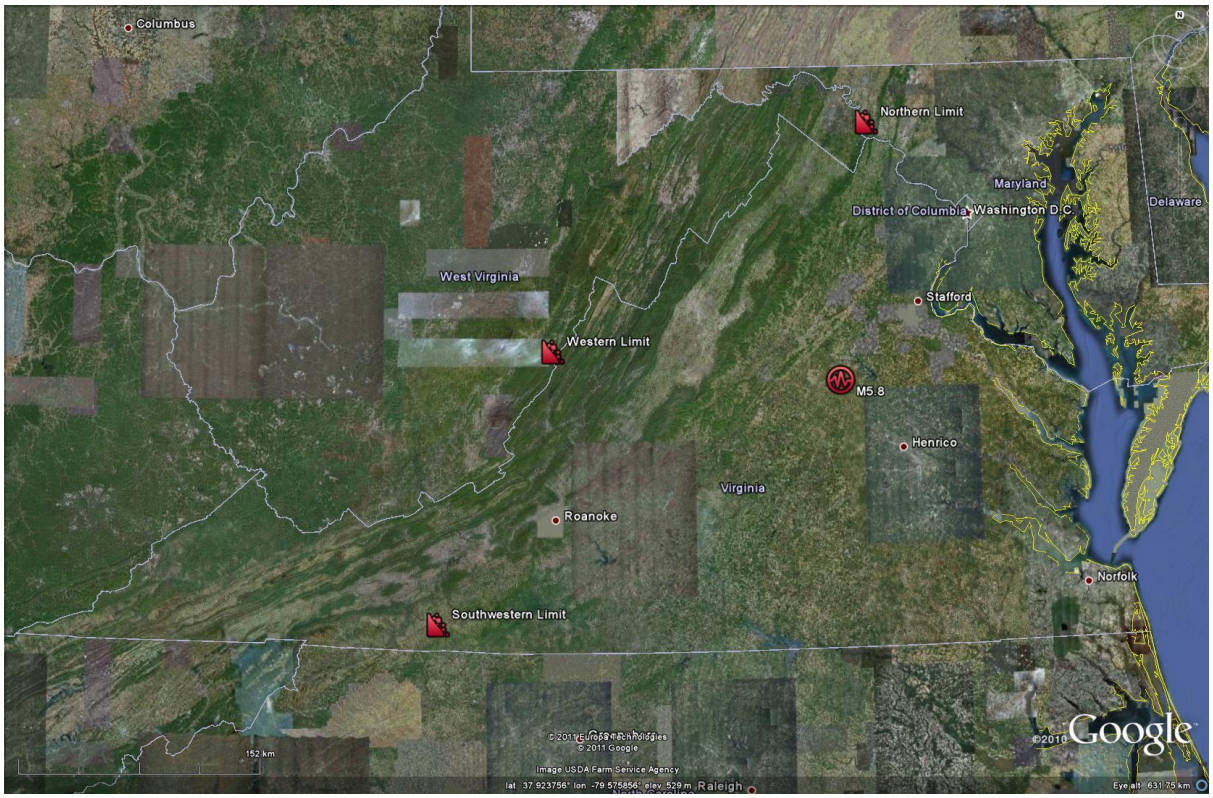

Figure 15. Aerial image showing the areal extent of rock falls to the North, West, and South of the epicenter; the eastern extent could not be determined.

Lifelines

Bridges

Numerous bridges in the epicentral region were given rapid inspections, with two bridges inspected in detail. The locations of the two bridges are shown in Figure 16. The first is the Yancyville Rd bridge, which in ~40 m long and crosses the S. Anna River in the NW-SE direction. We inspected this bridge in detail because it is very near where the liquefaction features were found in the riverbed and along the roadside. Photos of the bridge are shown in Figure 17. The bridge has a two lane concrete deck that sits on two bents, in addition to the NW and SE abutments. The only effects of the earthquake that could be found was ~2.5 cm gap between the soil and the SE pier (Figure 17b). The gap is shown in Figure 17c and was on the river side of the piers. It is uncertain whether the gap was due to movement of the pier due to earthquake shaking (i.e., movement of the bridge in the NW direction relative to the ground) or due to slumping of the river bank. No other evidence of slumping of the river bank near the bridge was observed

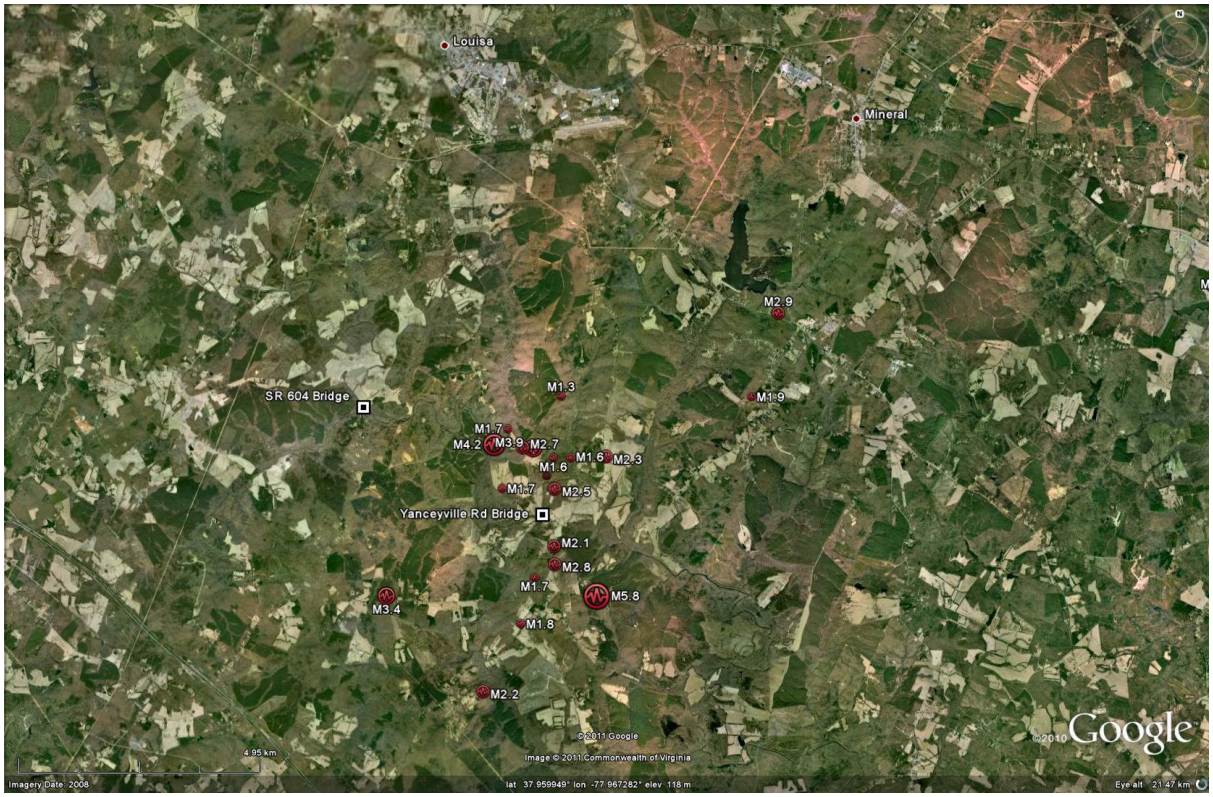

Figure 16. Aerial image showing the locations of the two bridges that were inspected in detail.

(a)

(b)

(c)

Figure 17. Yanceyville Rd Bridge (37.93898, -77.98269): (a) photo of the bridge looking to the NW; (b) photo of the SE bridge bent; and (c) photo of ~2.5 cm gap between one of the SE piers and soil (riverside only).

The second bridge that was inspected in detail was the SR 604 bridge, the location of which is shown in Figure 16. This bridge is ~36 m long and crosses the S. Anna River in the NE-SW direction. We inspected this bridge in detail because some of the local residents reported that "bumps" in the road surface of the abutment approaches worsened as a result of the main shock and aftershocks. Photos of the bridge are shown in Figure 18. As with the Yanceyville Rd bridge, this bridge has a two lane concrete deck that sits on two piers, in addition to the NE and SW abutments. Drawings obtained by Mark Carter, USGS, from the VDOT show that the abutments are founded on ~2.75 m (9 ft) of brown sandy silt with an SPT N-values of 5-7 blws/ft. Team members inspected the bridge on 24 August, the day after the main shock, but did not notice any obvious slumping of the abutments or evidence of seismic compression in the approaches (Figure 18a). However, after hearing from additional local residents that the bumps in the abutment approaches had gotten worse as a result of the main shock and aftershock, the bridge was revisited on 2 September, and it was found that the approaches already had been levelled and resurfaced (Figure 18b). Although heavy rains had fallen as a result of hurricane Irene, there was still evidence of a ~2.5 cm gap between SW pier and the soil on the riverside, shown in Figure 18f. As with the Yanceyville Rd bridge, it is uncertain whether the gap was due to movement of the pier due to earthquake shaking (i.e., movement of the bridge in the NE direction relative to the ground) or due to slumping of the river bank. Also, there was ~2.5 cm gap between the bridge deck and the SW abutment, shown in Figure 18e. It is likely that this existed prior to the earthquake to allow thermal expansion of the bridge deck.

(a)

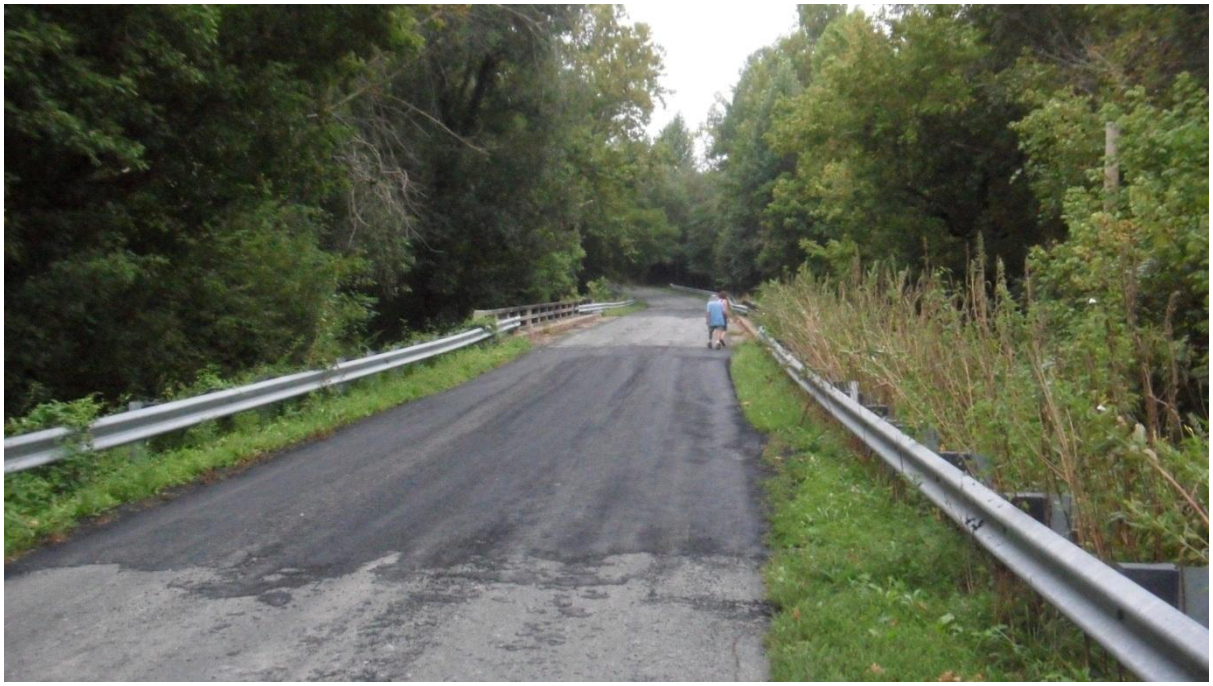

(b)

(c)

(d)

(e) (f)

Figure 18. SR 604 bridge (37.95915, -77.98269): (a) small bump in the approach to the bridge possibly due to seismic compression; (b) approach after relevelling and resurfacing of the bridge; (c) side view of bridge; (d) bridge abutment; (e) ~2.5 cm gap between bridge deck and the SW abutment; and (e) ~2.5 cm gap between the SW pier and soil (riverside only).

Power

Approximately 3000 customers lost power as a result of the main shock. However, virtually all the power was restored within 4 hrs after the event. Team members inspected the Cuckoo Substation on Jefferson Hwy, the location of which is shown in Figure 19 and photo of the substation shown in Figure 20a. The only evidence of the earthquake shaking on the substation was that a green metal equipment box slid ~2.5 cm to the north, as shown in Figures 20b,c. The box was not anchored to the concrete base slab.

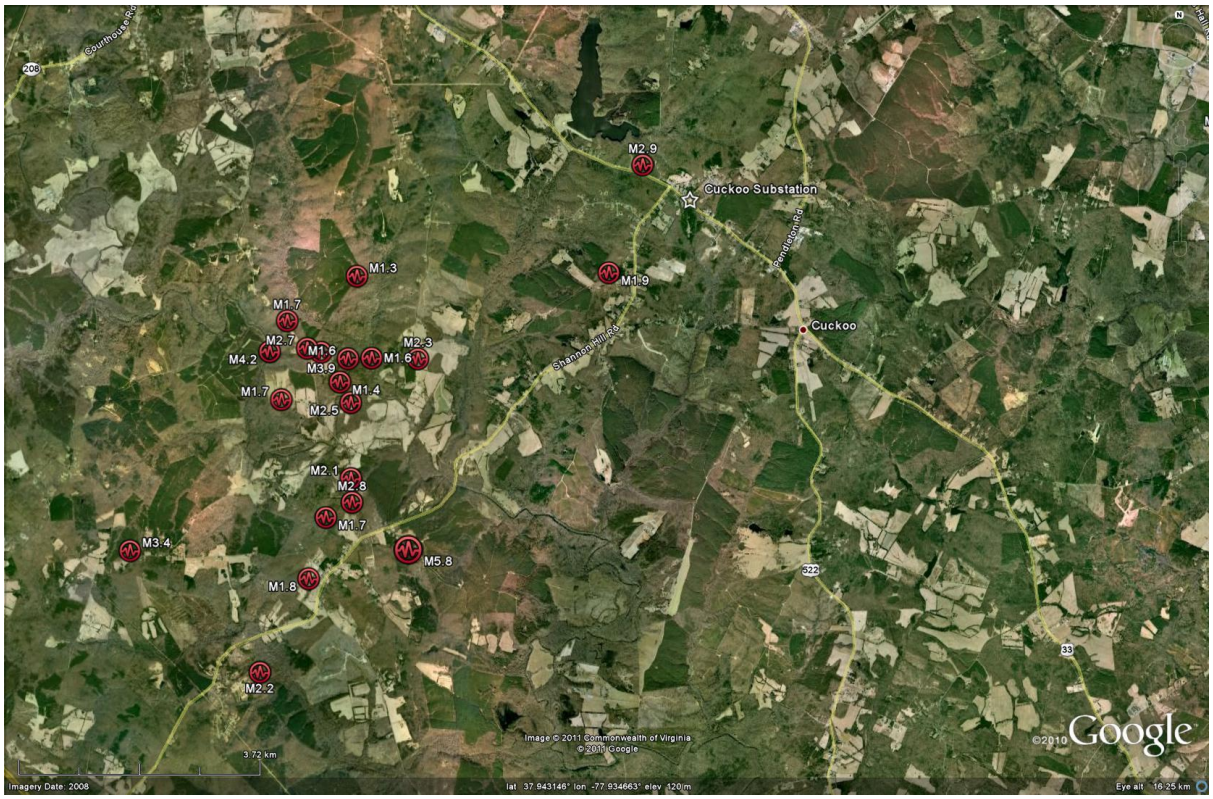

Figure 19. Aerial image of the epicentral region showing the location of the Cuckoo Substation, as well as the locations of the epicenters of the mainshock and aftershocks that occurred within two days of the mainshock.

(a)

(b)

(c)

Figure 20. Cuckoo Substation (37.97058, -77.91917): (a) photo of substation; (b) photo showing ~2.5 cm movement of green metal equipment box to the North; and (c) photo showing ~2.5 cm movement of the green metal equipment box to the North.

Pipelines

There were no reported gas leaks as a result of the earthquake. However, a 5 cm dia. water main in Mineral broke as a result of the earthquake, the location of which is shown in Figure 21. A photo of the excavated trench used to access the broken main is shown in Figure 22a. As may be observed in Figure 22b, the valve was heavily corroded and would have likely eventually failed even without the occurrence of the earthquake.

Figure 21. Aerial image of Mineral showing the location of the water main that broke during the earthquake.

(a)

(b)

Figure 22. Water main break in Mineral (38.01215, -77.90903): (a) trench showing broken water main; and (b) corroded water main value with a crack that was caused by the earthquake.

Railroad

Team members talked with a crew on 24 August who were replacing ties on the railroad tracks in Louisa (Figure 23). The crew chief said that coal trains run about every two hours but were suspended after the main shock until the tracks could be inspected. He said that no damage was found and the ties were being replaced due to age, not due to earthquake damage.

Figure 23. Crew replacing railroad old ties (38.019538, -77.978724).

Dams

Team members inspected seven dams in the epicentral region and an eighth dam in Bedford County, which is located ~150 km from the epicenter of the main shock. The locations of the dams are shown in Figure 24. The dams ranged widely in size, with the largest being the Lake Anna dam, which is a large dam with a small hydroelectric plant, and the smallest being the Pendleton House dam, which impounds a small pond. Photos/drawings of the inspected dams are shown in Figures 25-34, but only the Yancey Mill Dam and the Elk Lake Dam showed damage. With the exception of the Lake Anna Dam, no commentary is given in this report on the dams that didn't sustain any damage, rather only photos are shown.

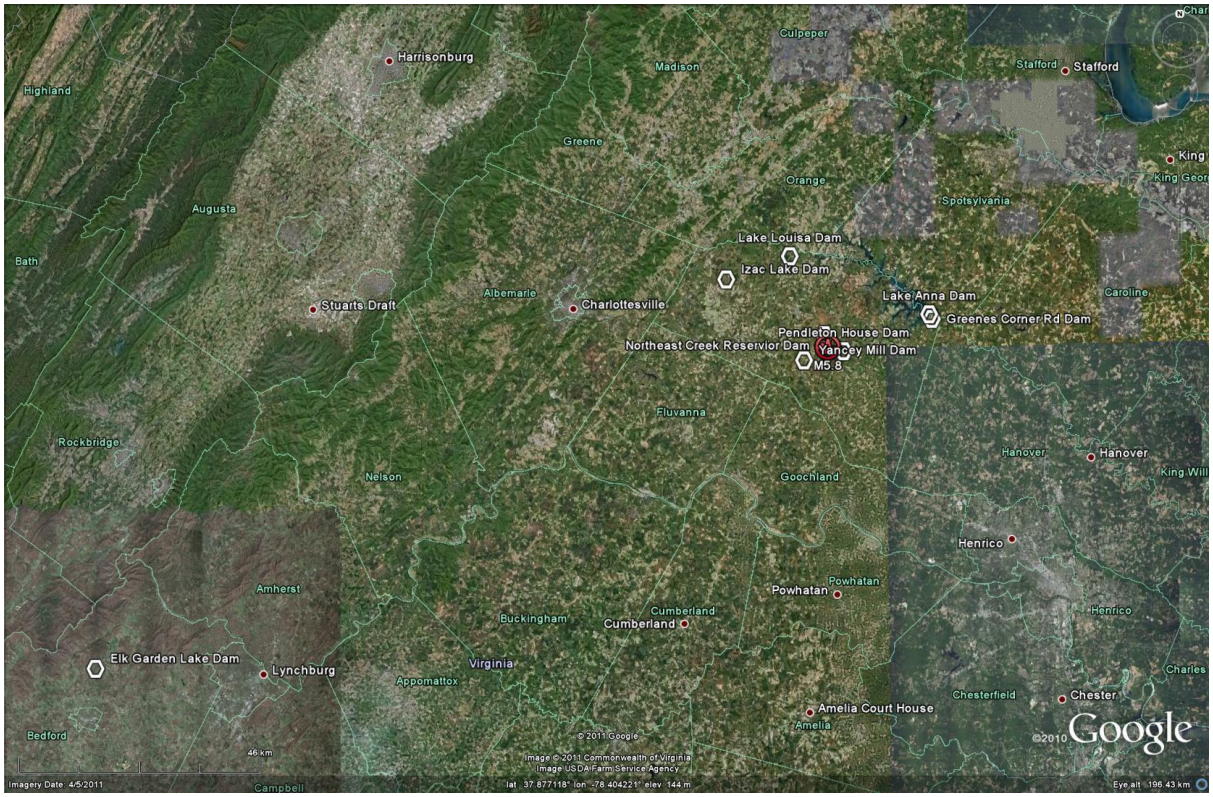

(a)

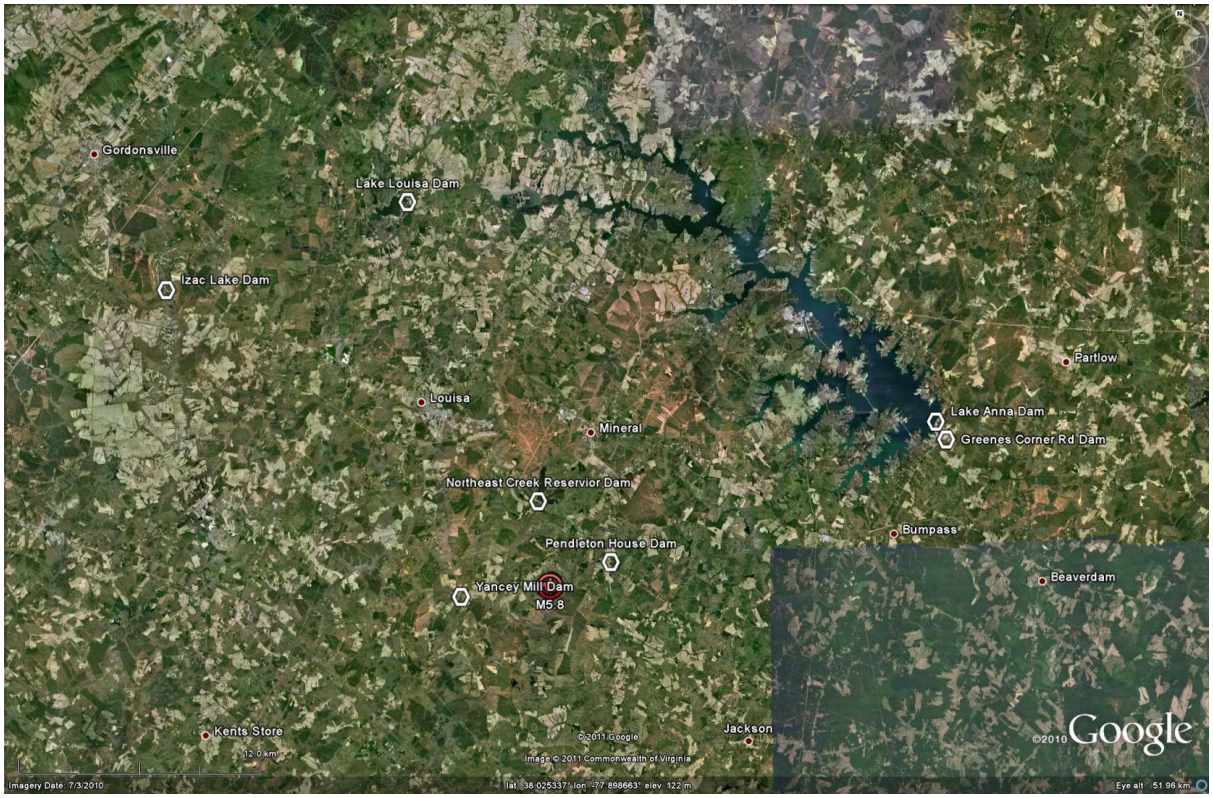

(b)

Figure 24. Aerial images showing dams that were inspected: (a) all dams inspected; and (b) dams inspected in the epicentral region.

Lake Anna Dam

The North Anna Dam was built in conjunction with the North Anna [Nuclear] Power Station (NAPS) and is jointly owned by Dominion Resources, Inc. and Old Dominion Electric Cooperative. The main dam is ~1,524 m (~5,000 ft) long and ~27 m (~90 ft) high and impounds Lake Anna, which is approximately 13,000 acres in surface area and approximately seventeen miles long. The main dam consists of a compacted earthen embankment, a concrete spillway, and two hydroelectric units, 220 kW and 740 kW, where the two hydroelectric units were added ~15 years after the completion of the dam. (Dominion, 2011)

Site selection and the design of the dam were completed in 1969, with construction of the dam beginning in late 1969 and completed in late 1972. Because Lake Anna serves as a secondary source of cooling water for the NAPS, the US Nuclear Regulatory Commission (NRC) served as the regulator for the design and construction of the dam. Accordingly, a relatively rigorous quality control/quality assurance (QC/QA) process was established during the design and construction of the dam. Plan and cross-sectional views of the dam are shown in Figure 25, where the cross-sectional view is for Sta. 22+00 which is the highest portion of the dam, as measured from baserock. (Dominion, 2011)

Because the Lake Anna serves as a secondary source for cooling water for the NAPS, the dam was designed to the same Design Basis Earthquake (DBE) as the NAPS. The DBE for the NAPS was assumed equal to the largest shock associated with the Arvonia Syncline, only with the epicenter of this event occurring at the site of the NAPS. The largest event associated with the Arvonia Syncline occurred on 22 December 1875 just west of Richmond, Virginia, had a maximum Modified Mercalli Intensity (MMI) of VII (Figure 26a), and had an estimated magnitude of 4.5. The peak horizontal ground acceleration (PGA) for rock sites was estimated to be less than 0.12 g. Accordingly, the PGA for the DBE for rock sites was assumed to be 0.12 g. To define the entire response spectrum for the DBE, an envelope was taken of the response spectra for the east-west and north-south components of the M_w6.0, 31 October 1935 (18:38) Helena, Montana earthquake and the south-east component of the Golden Gate record of the M_w5.28, 22 March 1957 San Francisco, California earthquake scaled to 0.12 g. The resulting 5% damped DBE response spectrum is shown in Figure 26b. However, although the response spectrum for the DBE was developed from motions recorded during the 1935 Helena and 1957 San Francisco earthquakes, time history analyses of the North Anna Dam were performed using the north-south component of the M_w6.95, 19 May 1940 Imperial Valley (El Centro) earthquake scaled to 0.12 g. The 5% damped response spectrum for this latter event is also shown in Figure 26b. (Dominion, 2009, 2011)

Motions from the 2011 Mineral, Virginia earthquake were recorded by a seismograph located on the basemat of the containment structure for Unit 1 of the NAPS, where the basemat is founded on rock. This seismograph is ~23 km from the epicenter of the event and ~8.5 km NW of the North Anna Dam; the dam is ~26 km from the epicenter. Assuming that the motions recorded at the NAPS were similar to those experienced at the North Anna Dam, the authors rotated the recorded motions to obtain motions that were oriented transverse to the longitudinal axis of the dam. The 5% damped response spectrum for these motions are shown

in Figure 26b. As may be observed from this figure, the motions from the Mineral earthquake exceed those of the DBE for oscillator frequencies greater than ~1.2 sec. Despite the DBE being exceeded over a wide range of frequencies, the team inspected the dam on 2 September 2011 and could not see any evidence of distress to the dam from the earthquake (Figure 27).

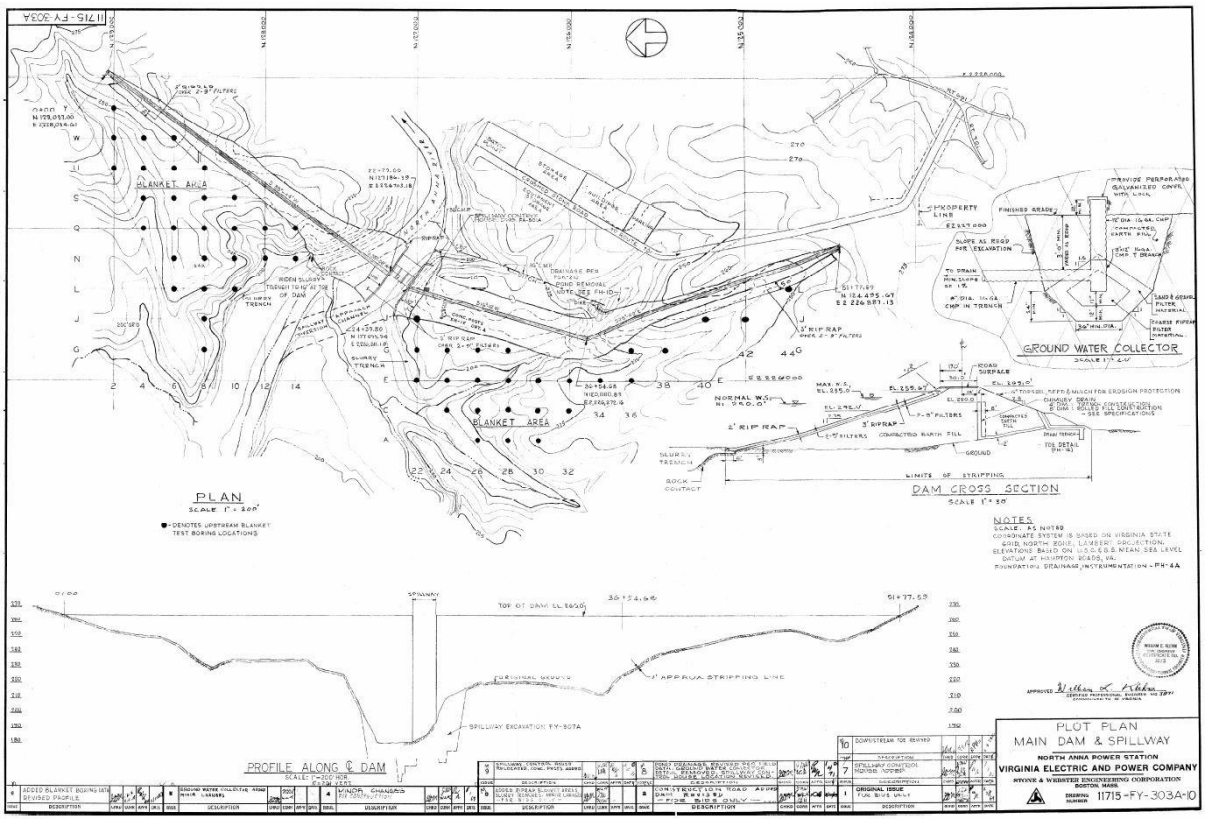

(a)

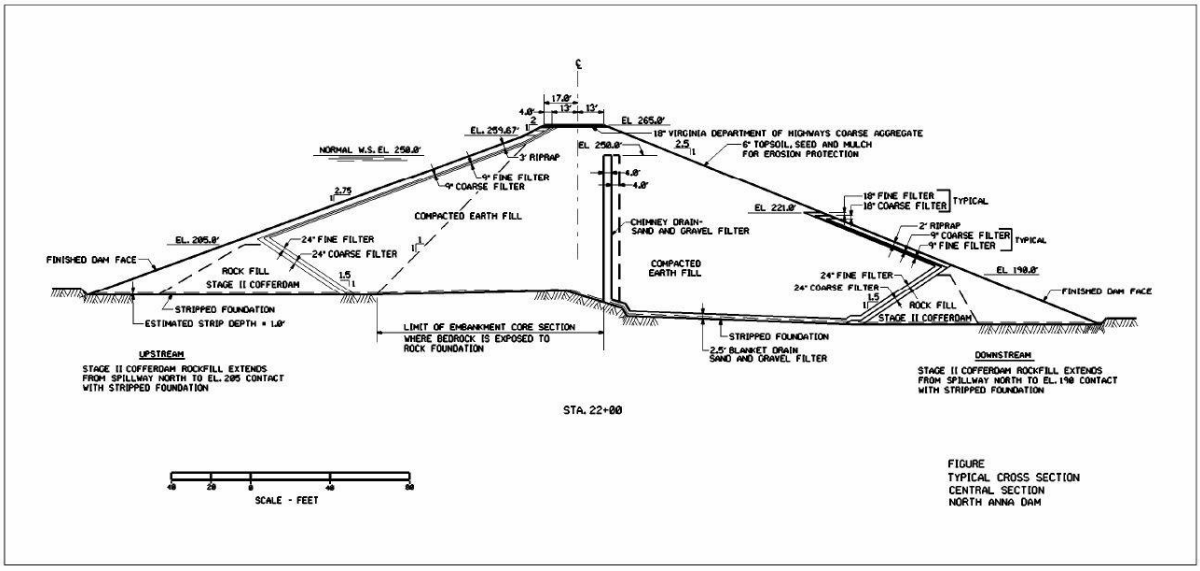

(b)

Figure 25. North Anna Dam: (a) plane view of dam layout; and (b) sectional view of the highest section of the dam, relative to baserock. (Dominion, 2011)

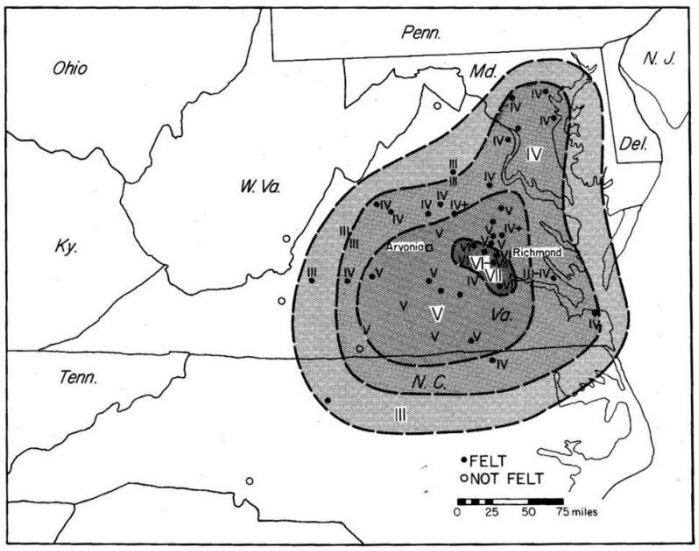

(a)

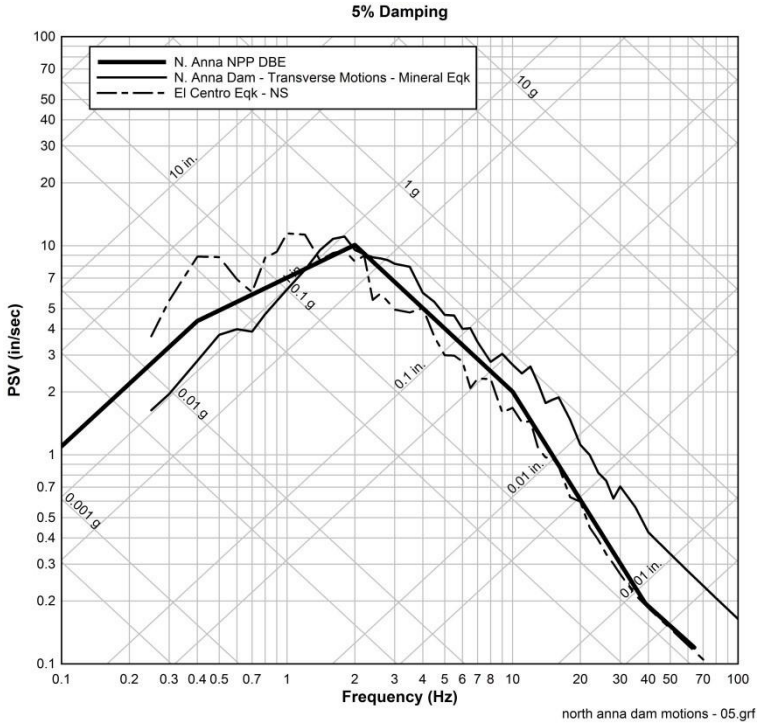

(b)

Figure 26. Design Basis Earthquake (DBE) for the North Anna Dam: (a) ~M_w4.5, 22 December 1875 earthquake, which is the largest historic event associated with the Arvonia Syncline (Chapman, 2012b); and (b) DBE, response spectrum for the 1940 El Centro N-S component scaled to 0.12 g, and response spectrum for the 2011 Mineral earthquake oriented in the transverse direction to the longitudinal axis of the dam.

(a)

(b)

(c)

(d) (e)

(f)

(g)

Figure 27. Lake Anna hydroelectric dam. (a) 38.00621, -77.71210. (b) 38.01739, -77.70918. (c)(d)(e)(f) 38.01315, -77.71297. (g) 38.01259, -77.71347.

Northeast Creek Reservoir Dam

(a)

(b)

(c)

Figure 28. Northeast Creek Reservoir Dam (37.98087, -77.93952).

Lake Louisa Dam

(a)

(b)

(c)

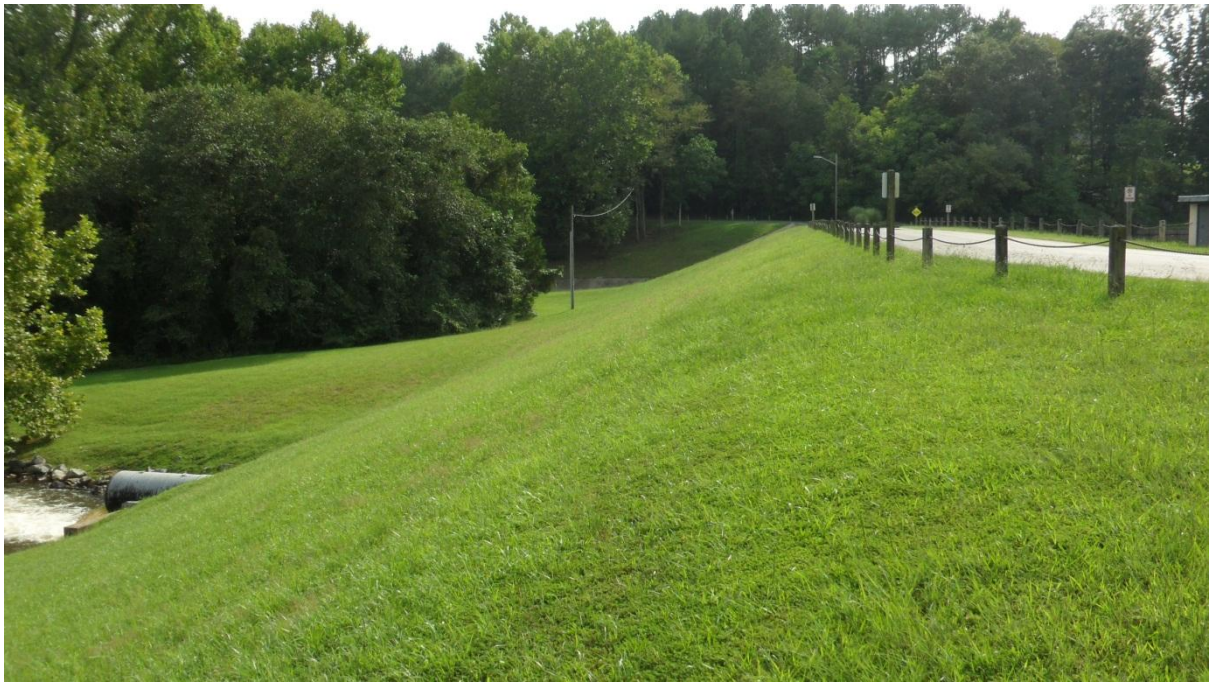

(d)

(e)

Figure 29. Lake Louisa dam and outflow (38.11439, -78.01041).

Izac Lake Dam

(a)

(b)

(c)

(d)

(e)

(f)

Figure 30. Izac Lake dam (38.07649, -78.14759).

Greenes Corner Road Dam

(a)

(b)

(c)

(d)

Figure 31. Greenes Corner Road Dam (38.00511, -77.70724).

Pendleton House Dam

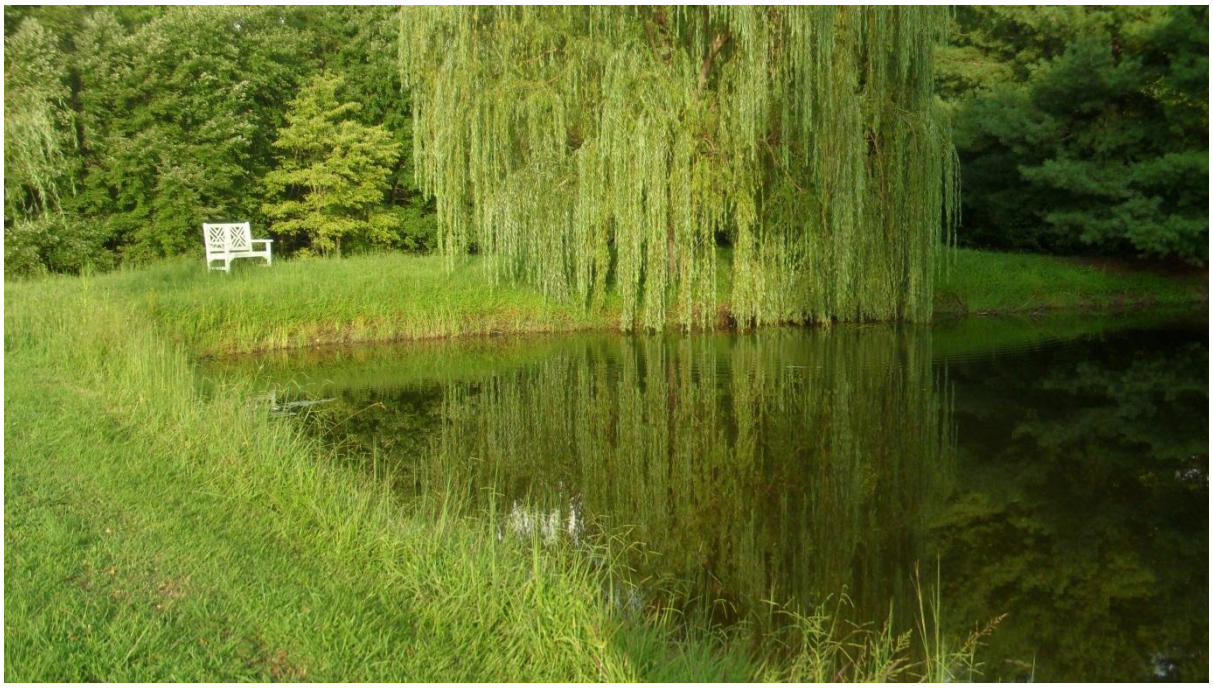

(a)

(b)

Figure 32. Pendleton House Dam (37.95283, -77.89812).

Yancey Mill Dam

The Yancey Mill Dam is on the S. Anna River and is a few meters upstream of the earthquake-induced sand boils found in the riverbed and nearby roadside ditch. The dam is ~1.5 m high. A photo of the dam in shown in Figure 33, and as shown in this photo, the dam is comprised of log cribs filled with rubble. A few of the cribs on the downstream face of the dam were broken and rubble spilled out. It is uncertain whether this damage was caused by the earthquake or not. A team member contacted the owner of the dam, and he said he wasn't aware of any pre-earthquake damage to the dam.

Figure 33. Yancy Mill Dam. It is unknown whether the damage shown in this photo resulted from the earthquake, but the owner was not aware of any pre-earthquake damage to the dam (37.93825, -77.98300).

Elk Garden Lake Dam

The Elk Garden Lake Dam is located in Bedford County, ~150 km from the epicenter of the main event. The dam is 9.1 m high and has a normal pool capacity of 66 acre feet. One of the homeowners near the dam was weed eating the downstream toe of the dam before the earthquake occurred. He noticed that a scarp started to form on the downstream face of the dam, near the crest. As a result, he stopped weed eating and went home, at which time the earthquake occurred. When he returned to the dam, the scarp had gotten bigger. The shallow slide is oval shaped and is ~6.4 m wide (running along the long axis of the dam) and ~9.1 m long (running down the downstream face of the dam). After the earthquake, the head scarp was ~17.8 cm high. There are no cracks visible at the top of the dam. The center of the slip is ~6.1 m to the left of the principal spillway pipe, looking downstream.

A team member met with W. Gray, the president of the homeowners association that owns the dam, on 9 September and inspected the dam. W. Gray said that 3 days before the earthquake they had 17.8 cm of rain in 12 hours. The saturated ground conditions likely triggered the initiation of the slide that occurred while the homeowner was weed eating, with the earthquake shaking making the slide worse. W. Gray said they covered the slide shortly after the earthquake with a plastic sheet to prevent water from flowing into the scarp. Photos of the slide taken both before and after it was covered with the plastic sheet are shown in Figure 34.

(a)

(b)

(c)

(d)

(e)

(f)

(g)

Figure 34. Shallow slide in the Elk Garden Lake Dam (37.4223, -79.5009): (a) photo of the shallow slide on the downstream face of the dam; (b) closer view of the shallow slide on the downstream face of the dam; (c) photo of head scarp of slide; (d) photo of slide taken from downstream toe of the dam; (e) photo showing head scarp covered with plastic sheet; (f) closer view of plastic sheet covering the head scarp; and (g) photo of plastic sheet taken from downstream toe of dam.

Landfill

The Louisa County landfill was inspected on 9 September. It is located ~10 km from the epicenter of the main shock as shown in Figure 35. A team member talked with R. Petty, who is the operations manager for the landfill and who was present at the landfill during the earthquake. R. Petty said he noticed a small crack on the front slope of the landfill immediately after the earthquake. The crack was ~2.5 cm wide, but R. Petty was uncertain whether it was there prior to the earthquake. Photos of the front slope of the landfill are shown in Figure 36. By the time R. Green visited the landfill, the crack had largely filled in as a result of the heavy rains from hurricane Irene. However, the crack looked like it was the scarp of a shallow slide in the temporary clay cover; remnants of the crack are shown in Figure 37.

R. Petty said he was checking a leachate monitoring well on the side of the landfill when the earthquake occurred and that the shaking caused the ground to soften considerably, to the point that he thought he was going to sink into the ground. A photo of the leachate monitoring well is shown in Figure 38. The ground around the well is soft clay.

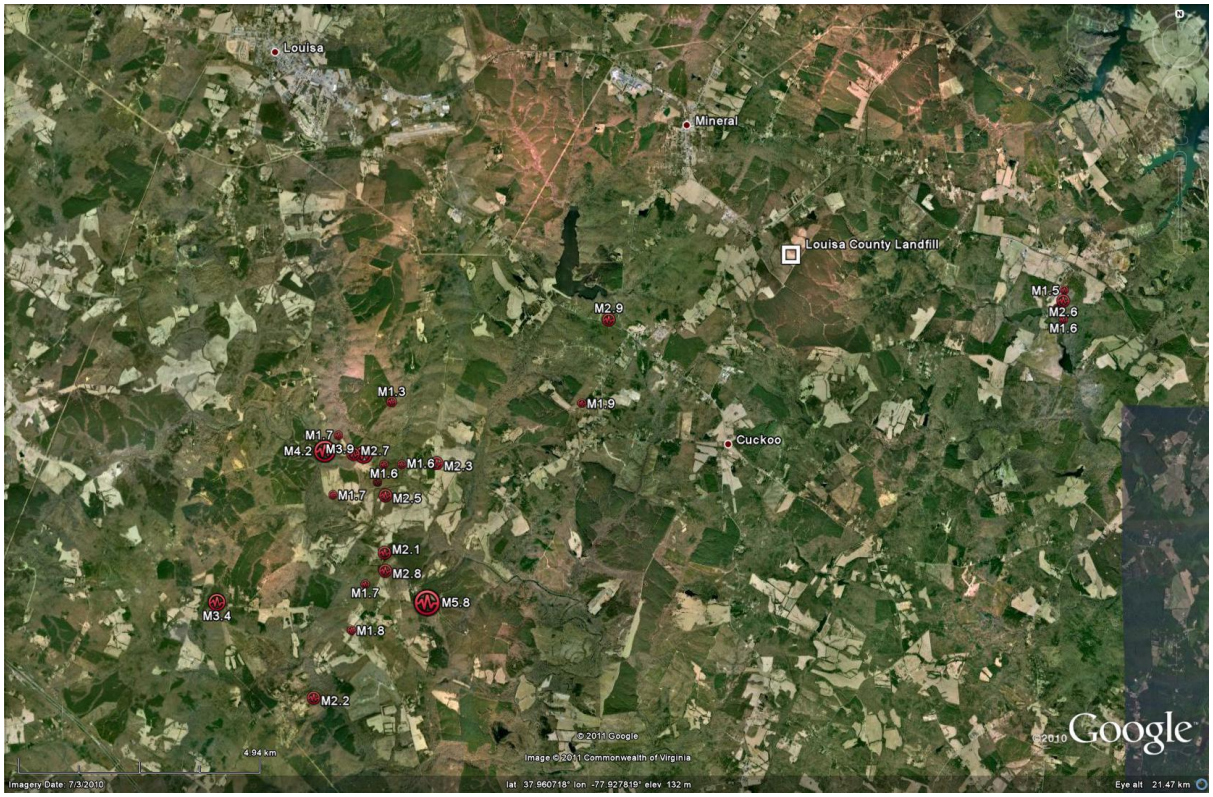

Figure 35. Aerial image showing the location of the Louisa County landfill.

(a)

(b)

Figure 36. Photos of the front slope of the Louisa County landfill (37.98670, -77.88474).

(a)

(b)

Figure 37. Photos showing the remnants of a crack in the front slope of the landfill that might have formed as a result of the earthquake shaking.

Figure 38. Leachate monitoring well where R. Petty was standing during the earthquake. The soft clay around the well got softer as a result of the earthquake shaking.

Public Buildings

Several public buildings in Louisa County were inspected on 23 and 24 August. The buildings included the Louisa Town Hall, Louisa County High School, Mineral Town Hall, US Post Office, Mineral, and Thomas Jefferson Elementary School. The locations of these buildings are shown in Figure 39. Also shown in this figure are contours developed by M. Heller, VA Department of Mines, Minerals, and Energy (DMME), and M. Carter (USGS) of severity of earthquake damage. The green contour shows the extent of minor damage, the

yellow contour shows the extent of minor-to-moderate damage, the orange contour shows the extent of moderate damage, the salmon contour shows the extent of moderate-to-major damage, and the red contour shows the extent of severe damage.

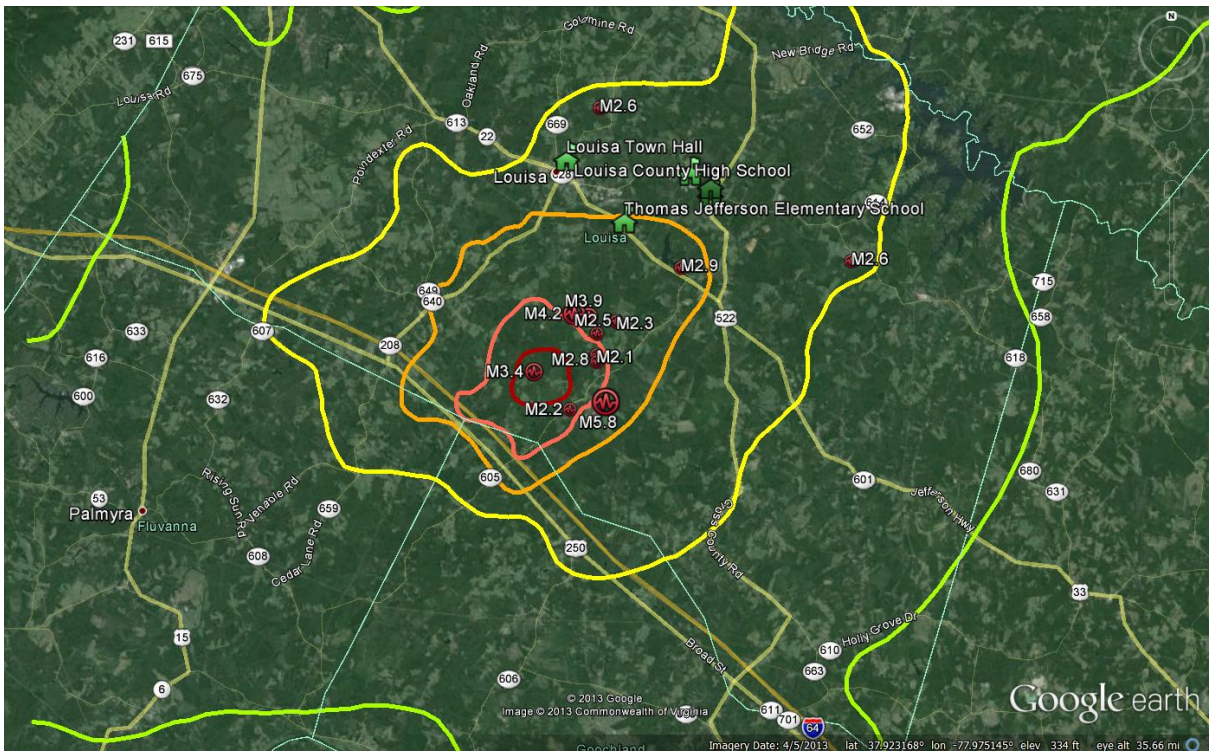

Figure 39. Aerial image showing the public buildings that were inspected after the earthquake (after Heller and Carter, 2014).

Schools

Louisa County High School

Team members inspected the Louisa County Public School Administration Building and the Louisa County High School on 23 August, about 6 hrs after the main shock and about a half hour after a M_w4.2 aftershock. The two buildings are located in the same complex, ~0.5 km apart. The Administration building only had minor cracking in the walls, but the internal contents of the building were in complete disarray. Photos of some offices in the Administration building are shown in Figure 40. The major axis of the building is in the NW-SE direction and the majority of the items that were tipped over were those along the NW and SE walls.

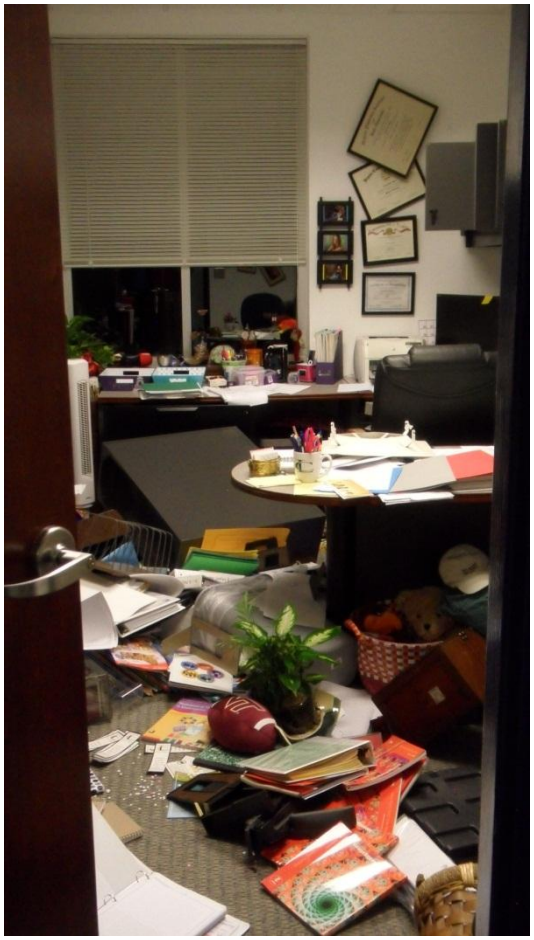

(a)

(b)

(c)

Figure 40. Typical damage to internal contents of offices in the Louisa County Public School Administration Building (38.02066, -77.92373).

The Louisa County High School building was built in sections over a period of several decades. The most severe damage to the building was in a portion that had a steel frame with concrete block infill walls and a brick façade; it is uncertain whether this same type of structural system was used in all sections of the building. The observed damage included cracks in the infill block walls, with blocks from the top of the walls falling through the dropped ceiling in places. Additionally, in many rooms ceiling tiles along opposite walls fell, indicating a pronounced direction of shaking; unfortunately, the orientations of the walls were not determined. As with the Administration building, the internal contents in many rooms were in disarray. Photos showing some of the damage in the High School building are shown in Figure 41.

(a)

(b)

(c)

(d)

(e)

(f)

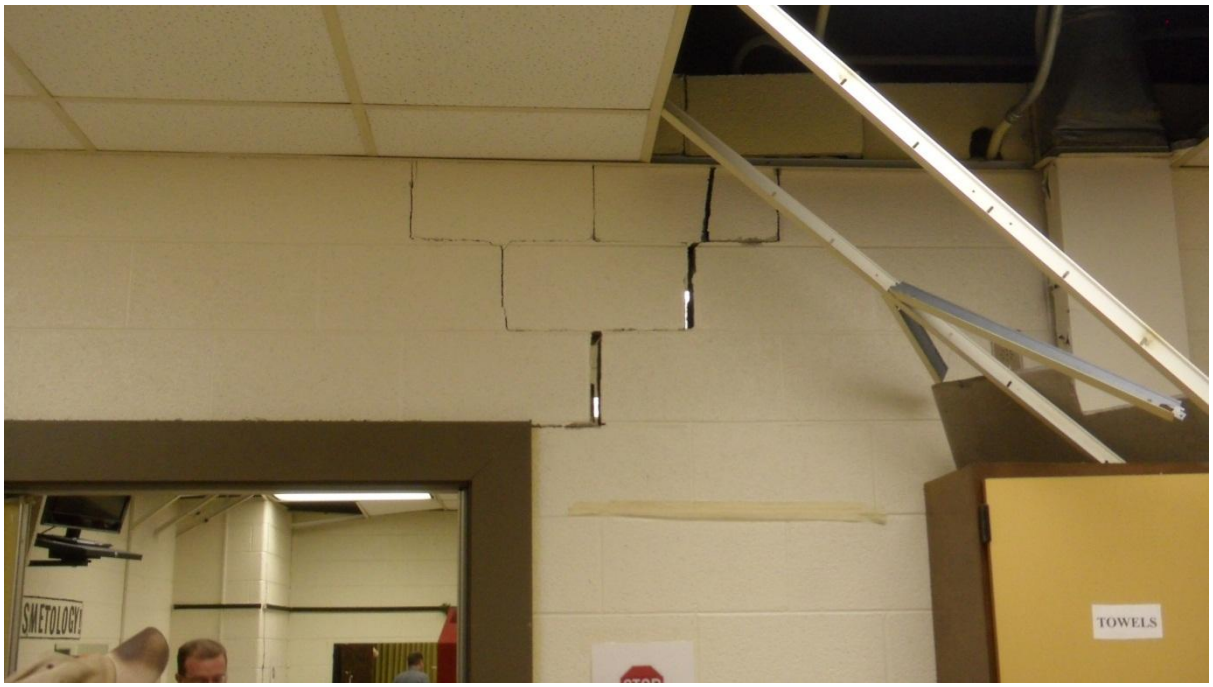

(g)

(h)

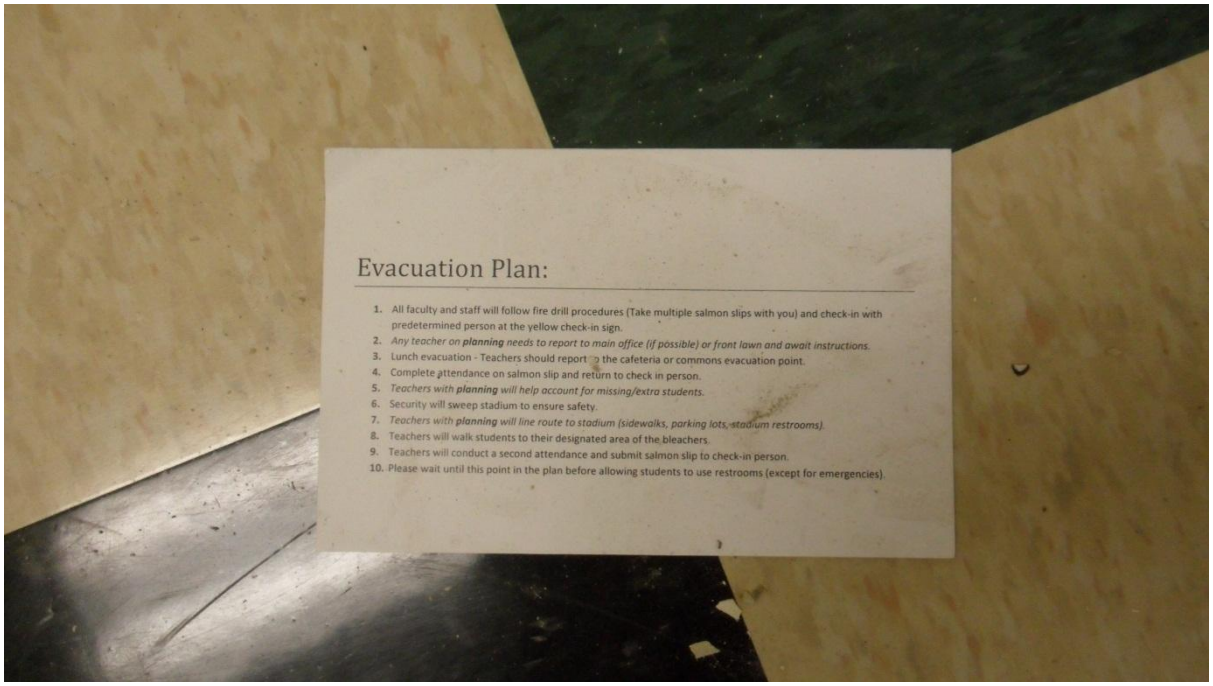
Evacuation Plan:
1. All faculty and staff will follow fire drill procedures (Take multiple salmon slips with you) and check-in with predetermined person at the yellow check-in sign.
2. Any teacher on planning needs to report to main office (if possible) or front lawn and await instructions.
3. Lunch evacuation - Teachers should report to the cafeteria or commons evacuation point.
4. Complete attendance on salmon slip and return to check in person.
5. Teachers with planning will help account for missing/extra students.
6. Security will sweep stadium to ensure safety.
7. Teachers with planning will line route to stadium (sidewalks, parking lots, stadium restrooms).
8. Teachers will walk students to their designated area of the bleachers.
9. Teachers will conduct a second attendance and submit salmon slip to check-in person.
10. Please wait until this point in the plan before allowing students to use restrooms (except for emergencies).

(i)

(j)

(k)

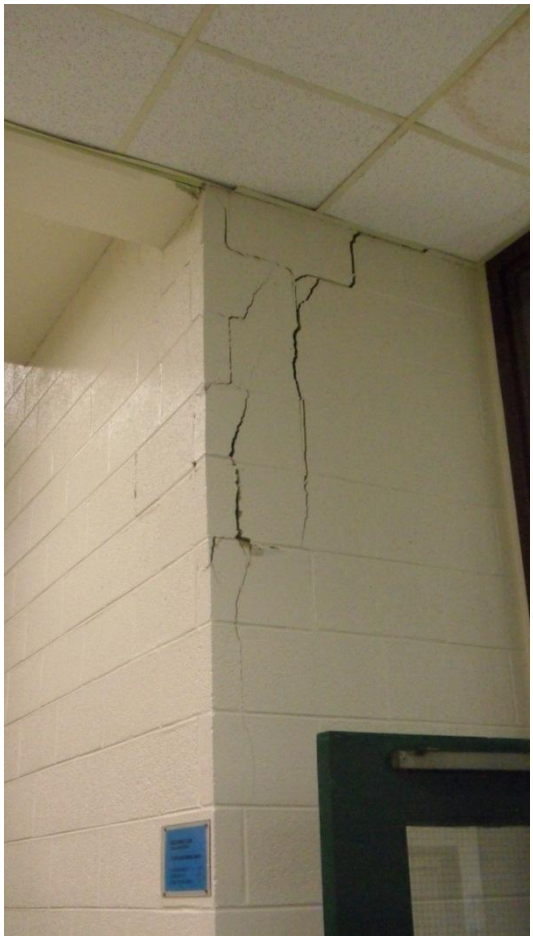

(l)

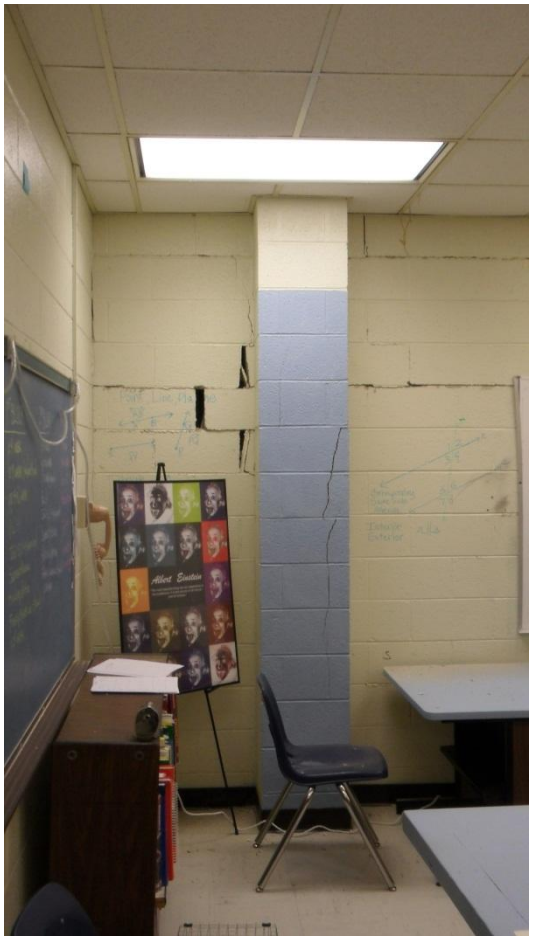

(m)

(n)

(o)

(p)

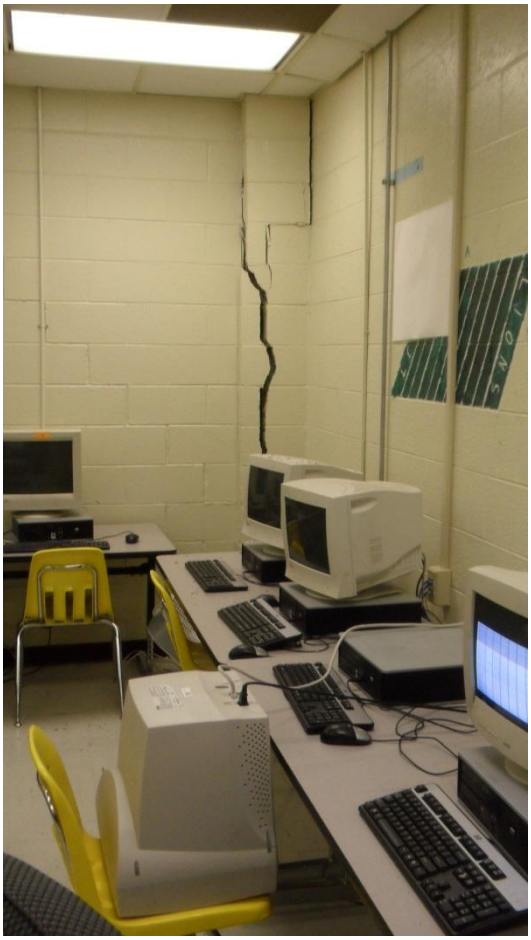

(q)

(r)

(s)

(t)

Figure 41. Typical damage to the Louisa County High School Building (38.01764, -77.92107).

Thomas Jefferson Elementary School

Team members visited Thomas Jefferson Elementary School on 24 August, but were only able to photograph the outside of the building. In addition to the Louisa County High School, this building was also severely damage by the earthquake. A photo of the outside of this building is shown in Figure 42.

Figure 42. Photo of the outside of Thomas Jefferson Elementary School (37.99468, -77.96233). Along with the LCHS, this building was severely damaged by the earthquake.

Town Halls

Louisa Town Hall

We had received reports on the night of the earthquake that the Louisa Town Hall (Figure 43) had a partial roof collapse. This prompted an inspection of the building on 24 August, the morning after the main shock. The building was constructed in 1907 (Figure 44a) and was damaged by fire in 1924 (Figure 44b); sometime between 1907 and 1924 a second story was added. The reports of damage were grossly exaggerated and most of the damage was cosmetic (e.g., fallen ceiling tiles, cracked plaster); photos of some of the damage are shown in Figure 45. The only structural damage was that the front wall of the building was slightly bowed outward as a result of the earthquake shaking.

Figure 43. Louisa Town Hall (38.02512, -77.99781) the morning after the earthquake.

(a)

(b)

Figure 44. Old photos of the town hall: (a) photo circa 1907 taken shortly after the building was constructed; and (b) photo circa 1924 taken after a fire gutted the structure.

(a)

(b)

(c)

(d)

(e)

(f)

(g)

(h)

Figure 45. Photos showing examples of damage to the Louisa Town Hall.

Mineral Town Hall

We had received reports on the night of the earthquake that the Mineral Town Hall had completely collapsed during the earthquake. This prompted team members to inspect the building on 24 August, the morning after the main shock. As with the Louisa Town Hall, the initial damage reports for the Mineral Town Hall were grossly exaggerated. A photo obtained from the internet believed to have been taken within hours after the earthquake on 23 August is shown in Figure 46. As shown in this figure, the damage was mainly limited to the brick parapet towards the back of the building. Photos taken by a team member on 24 August are shown in Figure 47. We did not inspect the inside of the building.

Figure 46. Photo of the Mineral Town Hall (38.01090, -77.90848) believed to have been taken within hours after the earthquake (source: internet).

(a)

(b)

(c)

Figure 47. Damage to the Mineral Town Hall (38.01090, -77.90848).

US Post Office, Mineral, VA

Team members inspected the US Post Office in Mineral on 24 August, the morning after the main shock. The post office was open when we visited, but the main entrance and foyer were closed and residents had to use the backdoor to pick up their mail. Figure 48 shows the damage to the brick façade to the main entrance to the building. As with the Louisa County High School, ceiling tiles along opposite walls fell in the Mineral Post Office. In this case the tiles along the North and South walls fell (Figure 49), indicating a pronounced N-S direction of shaking.

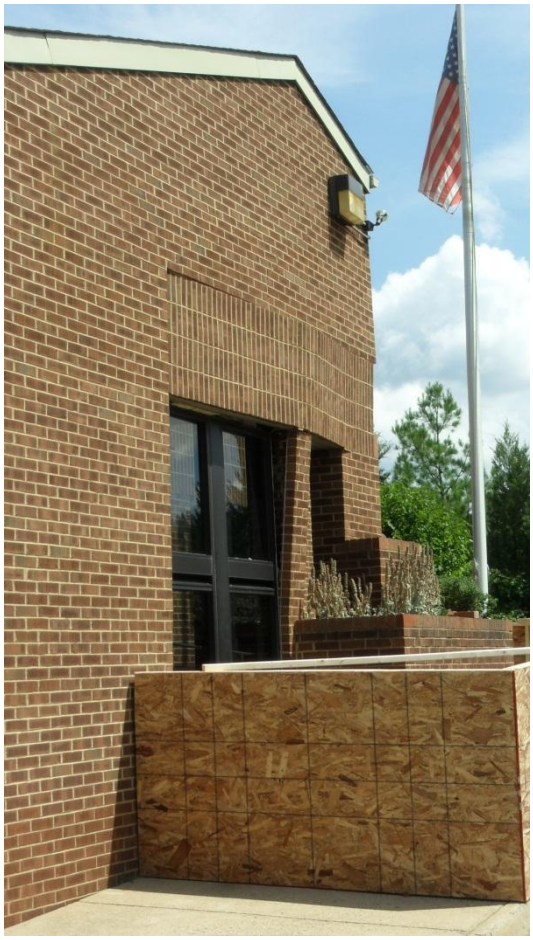

(a)

(b)

(c)

(d)

(e)

Figure 48. Damage to the main entrance of the Mineral Post Office (38.00669, -77.90859).

Figure 49. Ceiling tiles that fell along the North wall in the Mineral Post Office (38.00669, -77.90859).

Residential Structures

With M. Carter (USGS), team members inspected residential structures throughout the epicentral region. Most of the structural damage was constrained to unreinforced masonry, to include brick/block buildings and chimneys, block foundation walls, and brick façades. Figure 50 shows contours developed by M. Heller (DMME) and M. Carter (USGS) of damage severity in the epicentral region. The green contour shows the extent of minor damage, the yellow contour shows the extent of minor-to-moderate damage, the orange contour shows the extent of moderate damage, the salmon contour shows the extent of moderate-to-major damage, and the red contour shows the extent of severe damage. M. Carter noted that houses oriented with their long-axes close to either N-S or E-W sustained more damage than those oriented NE-SW/NW-SE. He also noted that structures on the sides of hills sustained more damage than those on the top of the hills, and structures at base of hills sustained even less damage. Figure 50 also shows the locations of several of the residential structures that we inspected.

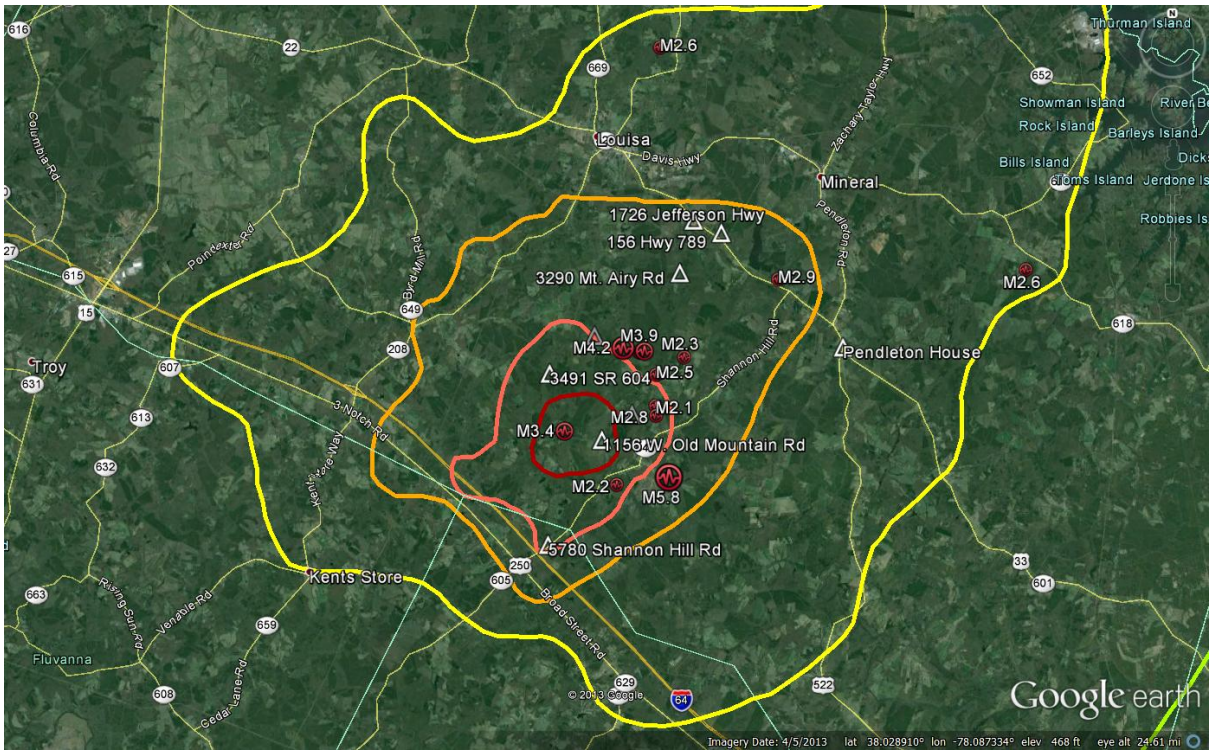

Figure 50. Aerial image of the epicentral region with contours of damage severity and the locations of residential structures that we inspected (after Heller and Carter, 2014).

3290 Mt. Airy Rd, Louisa

Figure 51. Typical damage to block foundation walls (37.9790, -77.9692).

1726 Jefferson Hwy, Louisa

Figure 52. Typical damage to brick chimneys (37.9966, -77.9631).

156 Hwy 789, Mineral

(a)

(b)

(c)

Figure 53. Representative severe damage to brick façade and block foundation walls (37.9923, -77.9513).

1156 W. Old Mountain Rd, Louisa

(a)

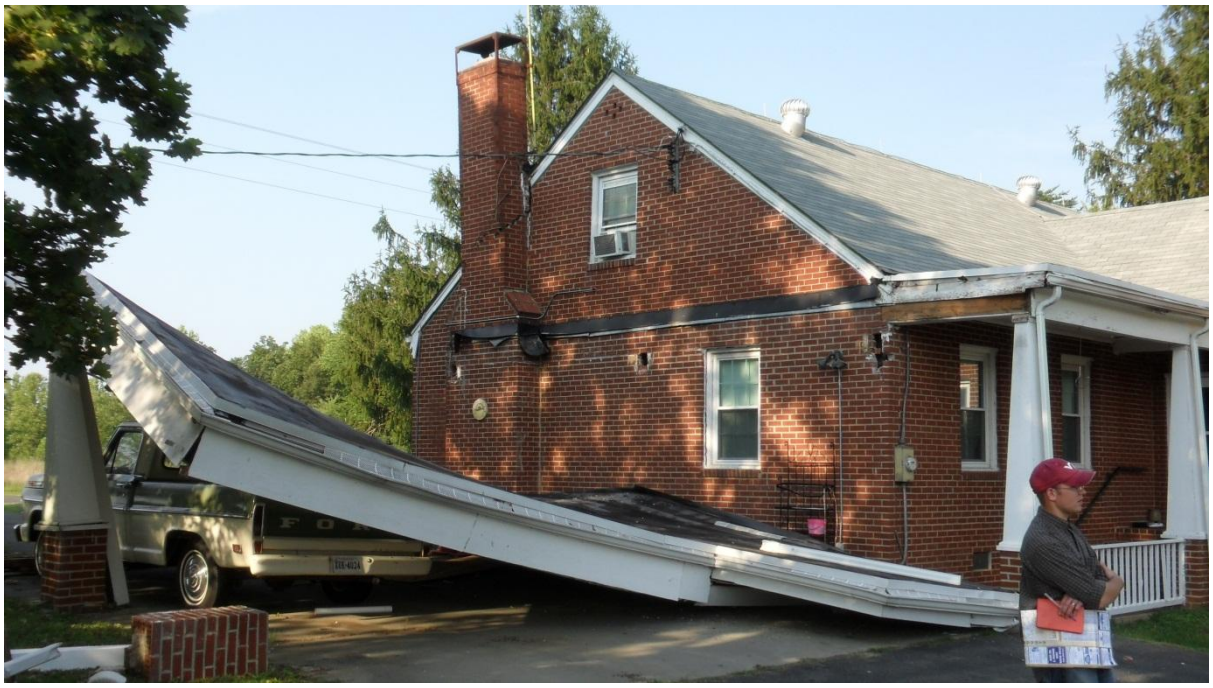

(b)

(c)

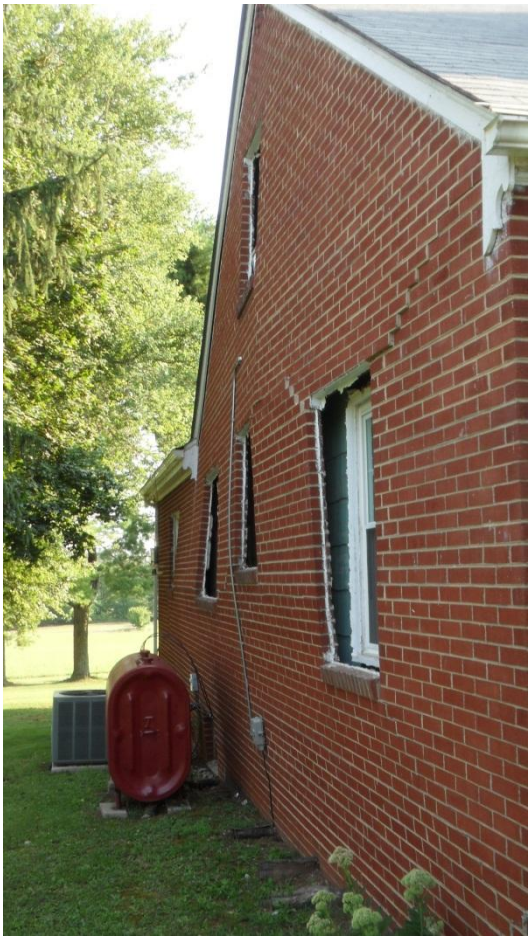

(d)

(e)

Figure 54. Representative severe damage to brick façade (37.9229, -78.0033).

3491 SR 604, Louisa

(a)

(b)

Figure 55. Typical damage to block foundation (37.9455, -78.0253).

5780 Shannon Hill Rd, Louisa

Figure 56. Representative severe damage to brick façade (37.8878, -78.0267).

Twin Oaks Commune

(a)

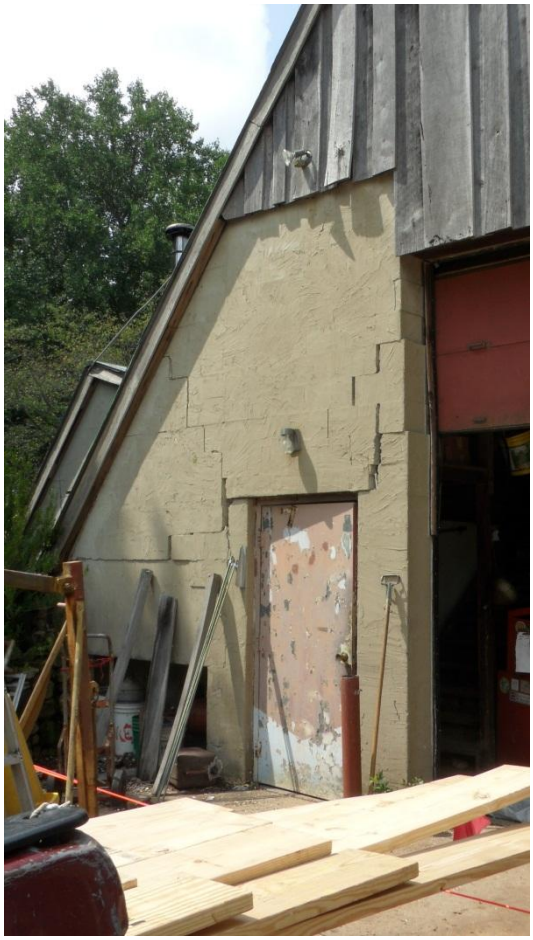

(b)

(c)

(d)

Figure 57. Damage to an unreinforced block garage structure (37.9314, -77.9903).

(a)

(b)

(c)

Figure 58. Damage to floor in dining facility (37.9306, -77.9898) caused by damage to unreinforced block foundation wall: (a) Crack in the tiled floor; (b) foundation wall below the crack in the tiled floor (note the broken block supporting the sill beam); (c) gap between sill beam and concrete block formed due to rotation of the sill beam resulting from the broken block supporting the sill beam.

Bend of River Rd

Team members inspected several houses on Bend of River Rd. The house shown in Figure 59 had a Superior Walls foundation system. The system consists of precast panels that are bolted together onsite. The owners of the house were home at the time of the earthquake and described the level of shaking as very intense. However, we could not find any damage to the foundation system.

(a)

(b)

(c)

Figure 59. Small house with a Superior Walls foundation system. We found no damage to the foundation system despite intense shaking. (37.95806, -78.00606)

Pendleton House

The Pendleton House was inspected on 26 August. The Pendleton House was completed in 1818 and is listed in the National Registry of Historic Places. Figure 60a is a photo obtained from the internet showing the house before the earthquake. The subsequent photos were taken on 26 August, after the earthquake. As may be observed from these photos, the brick chimneys and walls on both sides of the walls suffered significant damage. Team members were unable to inspect the inside of the house.

(a) (source: internet)

(b)

(c)

(d)

(e)

(f)

(g)

(h)

Figure 60. Pendleton House (37.95327, -77.89987), which is listed in the National Registry of Historic Places.

References

Ambraseys, N.N., 1988, Engineering Seismology, *Earthquake Engineering and Structural Dynamics*, 17, 1-105.

ASTM (American Standards for Testing of Materials), 2011, ASTM D2487-11: Standard Practice for Classification of Soils for Engineering Purposes (Unified Soil Classification System), ASTM International, West Conshohocken, PA.

Dominion, 2009, North Anna Power Station Units 1 and 2 Updated Final Safety Analysis Report, rev45, Virginia Electric and Power Company (Dominion), Richmond, VA.

Dominion, 2011, North Anna Dam, Supporting Technical Information Document, rev1, FERC Project No. 6335-VA, Virginia Electric and Power Company (Dominion), Richmond, VA.

Chapman, M.C., 2012b, Personal Communication with R. Green.

Green, R.A., Olson, S.M., Cox, B.R., Rix, G.J., Rathje, E., Bachhuber, J., French, J., Lasley, S., and Martin, N. 2011a, Geotechnical Aspects of Failures at Port-au-Prince Seaport During the 12 January 2010 Haiti Earthquake, *Earthquake Spectra*, 27(S1), S43-S65.

Green, R.A., Wood, C., Cox, B., Cubrinovski, M., Wotherspoon, L., Bradley, B., Algie, T., Allen, J., Bradshaw, A., and Rix, G., 2011, Use of DCP and SASW Tests to Evaluate Liquefaction Potential: Predictions vs. Observations During the Recent New Zealand Earthquakes, *Seismological Research Letters*, 82(6), 927-938.

Green, R.A., and Lasley, S., 2012, Liquefaction resulting from the 2011 central Virginia earthquake: Geological Society of America Abstracts with Programs. Vol. 44, No. 4, p. 14.

Heller, M.J. and Carter, A.M., 2014, Residential property damage in the epicentral area of the Mineral, Virginia, Earthquake of August 23, 2011, The August 23, 2011 Earthquake in Central Virginia and Its Significance for Seismic Hazards in Eastern North America (J.W. Horton et al., eds), GSA Special Paper, Geological Society of America, Boulder, CO. (*in review*)

Olson, S.M., Green, R.A., Lasley, S., Martin, N., Cox, B.R., Rathje, E., Bachhuber, J., French, J., 2011, Documenting Liquefaction and Lateral Spreading Triggered by the 12 January 2010 Haiti Earthquake, *Earthquake Spectra*, 27(S1), S93-S116.

Seed, H.B., Tokimatsu, K., Harder, L.F., and Chung, R., 1984, The Influence of SPT Procedures on Soil Liquefaction Resistance Evaluations, Report No. UCB\EERC-84/15, Earthquake Engineering Research Center, Univ. California, Berkeley, CA.

Skempton, A.W., 1986, Standard Penetration Test Procedures and the Effects in Sands of Overburden Pressure, Relative Density, Particle Size, Aging and Overconsolidation, *Geotechnique*, 36(3), 425-447.

Sowers, G.F. and Hedges, C.S., 1966, Dynamic cone for shallow in-situ penetration testing, vane shear and cone penetration resistance testing of in-situ soils. *ASTM STP 399, American Society of Testing Materials*, Philadelphia, PA, 29-37.

Tsuchida, H., 1970, Prediction and Countermeasure Against the Liquefaction in Sand Deposits, Abstract of the Seminar in the Port and Harbor Research Institute (in Japanese.

Youd, T.L., Idriss, I.M., Andrus, R.D., Arango, I., Castro, G., Christian, J.T., Dobry, R., Finn, W.D.L., Harder, L.F., Hynes, M.E., Ishihara, K., Koester, J.P., Liao, S.S.C., Marcuson III, W.F., Martin, G.R., Mitchell, J.K., Moriwaki, Y., Power, M.S., Robertson, P.K., Seed, R.B., and Stokoe II, K.H., 2001, Liquefaction resistance of soils: summary report from the 1996 NCEER and 1998 NCEER/NSF workshops on evaluation of liquefaction resistance of soils. *Journal of Geotechnical and Geoenvironmental Engineering, ASCE*, 127 (10), 817-833.